Calhoun: The NPS Institutional Archive

DSpace Repository

Theses and Dissertations | 1. Thesis and Dissertation Collection, all items

1967-06

An experimental investigation of a gas lubricated stepped sector thrust bearing at high bearing numbers.

Stumbo, Stanley Charles

Monterey, California. U.S. Naval Postgraduate School

http://hdl.handle.net/10945/12170

Downloaded from NPS Archive: Calhoun

http://www.nps.edu/library

Calhoun is the Naval Postgraduate School's public access digital repository for research materials and institutional publications created by the NPS community. Calhoun is named for Professor of Mathematics Guy K. Calhoun, NPS's first appointed -- and published -- scholarly author.

Dudley Knox Library / Naval Postgraduate School
411 Dyer Road / 1 University Circle
Monterey, California USA 93943

NPS ARCHIVE
1967
STUMBO, S.

AN EXPERIMENTAL INVESTIGATION OF A GAS LUBRICATED STEPPED SECTOR THRUST BEARING AT HIGH BEARING NUMBERS

STANLEY CHARLES STUMBO

AN EXPERIMENTAL INVESTIGATION OF A GAS [illegible] STEPPED SECTOR [illegible] AT HIGH BEARING NUMBERS

by

Stanley Charles [illegible]
Lieutenant, United States Navy
B.S., Naval Academy, 1960

[redacted]

Submitted in partial fulfillment of the
requirements for the degree of

MASTER OF SCIENCE IN MECHANICAL ENGINEERING

from the

NAVAL POSTGRADUATE [illegible]
June 1967

ARCHIVE
M80,S.

ABSTRACT

The existing analytical solutions for gas lubricated stepped sector thrust bearings are reviewed. An experiment performed at high bearing numbers (123 to 165) using air at atmospheric pressure is described. Results are presented of tests conducted using a bearing optimized by the methods of Ausman and Wildmann for high speed operation. Most of the design optimizations are confirmed for high bearing numbers; the exception is load carrying capacity. The load capacity curve obtained takes the same form as that predicted by theory but is lower for any given bearing number by a constant percentage. This points to a need for re-evaluation of determination of load carrying capacity.

TABLE OF CONTENTS

LIST OF TABLES

LIST OF FIGURES

NOMENCLATURE

A	Bearing area (in.^{2})
b	Radius ratio = r_i/R
h	Lubricating film thickness (in.)
h_1	Film thickness in leading edge region (in.)
h_2	Film thickness in trailing edge region (in.)
L	Load parameter = $W/p_a A$
n	Number of sectors
N	Rotation rate (rpm)
p	Pressure (psi)
q	Compression ratio = $h_1/h_2 = (\Delta + h_2)/h_2 = 1 + 1/\alpha$
Q	Mass flow rate (lbm./sec.-in.)
r	Radial coordinate (in.)
r_i	Bearing inner radius (in.)
R	Bearing outer radius (in.)
t	Time coordinate (sec.)
V	Velocity of fluid (in./sec.)
W	Bearing load (lbf.)
z	Axial coordinate (in.)
α	Minimum clearance ratio = h_2/Δ
Δ	Step depth (in.)
δ	Angular width of groove between thrust pads (degrees or rad.)
Λ	Bearing number = $\frac{6\mu\omega R^2}{p_a h_2^2}$
Λ_Δ	Bearing number based on step depth = $\frac{6\mu\omega R^2}{p_a \Delta^2}$
Λ'	Modified bearing number = $\Lambda(1-b^2)$
Λ'_Δ	Modified bearing number based on step depth = $\Lambda'_\Delta(1-b^2)$

γ	Sector arc length (degrees or radians)
η	Step ratio = τ/γ
ρ	Lubricant density (lbm./in.^{3})
θ	Coordinate angle (radians)
μ	Viscosity (reyns = lbf.-sec./in.^{2})
τ	Arc length of leading edge region (degrees or radians)
ω	Angular velocity (rad./sec.)

Subscripts

1	Refers to leading edge region
2	Refers to trailing edge region
a	Refers to ambient condition
r	Radial
θ	Circumferential
Δ	Refers to the step
opt	Optimized

ACKNOWLEDGEMENTS

Without the exceptional cooperation and assistance of AiResearch Corporation, Los Angeles, California, this investigation would not have been possible. The writer owes gratitude to Mr. A. Silver, Manager, Research and Development Laboratory for the arrangements he took the valuable time to make.

Thanks are also due to Professor P. F. Pucci for his valuable and skillful guidance.

The encouragement and help with typing by my wife, Bunny, contributed much to this effort. The excellent photographs are by Lieutenant J. A. Pethick, USN.

1. Introduction.

In a rapidly expanding technology, which creates demands for machinery components that will operate in progressively more severe or unusual environments, it is soon found that "conventional" lubricants for moving or rotating parts will no longer serve. Because they possess several unique advantages, gases are a logical consideration as a lubricant when seeking solutions to many design problems.

Gas lubricants are particularly attractive at extremely high or at very low temperatures. Since, in contrast to liquids, the viscosity of gases is relatively constant and even increases slightly with temperature, gas lubricants have an obvious application in very high temperature rotating machinery. At the other end of the scale, elements such as nitrogen and helium retain their desirable lubricating qualities at cryogenic temperatures. Indeed, the "boiloff" from liquified gases is often used as the lubricant for expansion turbine gas liquifiers.

Another important advantage of gas lubricated bearings is the extremely low power loss from friction at very high speeds. This, plus the fact that this power loss is relatively unvarying, dictates the use of gas bearings in precision applications such as high speed gyroscopes. The low friction loss at high speeds plus high temperature operation makes gas lubricated bearings the most desirable type for gas turbines and turbojet engines.

In many areas gas lubricants can solve the problem of contamination. When pumping, compressing, or expanding high purity gases or refrigerants, the use of the process fluid as a lubricant will prevent mixing of the fluid with oils or greases. In food processing machinery, elimination of petroleum lubricants prevents contamination of foods. In nuclear reactors,

it is desirable to eliminate oils, greases, and solid lubricants which break down or form radioactive isotopes when subjected to radiation.

As with conventional bearings, gas lubricated bearings fall into two major classes, self-acting, or hydrodynamic bearings, and pressurized, or hydrostatic bearings. There exists a wide variety of both journal and thrust type bearings in each class. Self-acting bearings are, in general, the least complex, requiring neither separate gas supplies and piping nor fluid passages and orifices to complicate the design of a machine.

Unfortunately, gas lubricated bearings have only recently emerged from the realm of laboratory curiosities. Currently most types are subject to serious instabilities and require extremely close machining tolerances with very smooth finishes. Air film thicknesses are so small that thermal distortions are a major cause of failures. To gain a better understanding of the capabilities and problems of gas lubricated bearings, this project was undertaken.

Because of an interest developed while the author was working at AiResearch Manufacturing Company on a summer industrial tour, this study will be confined to self-acting thrust bearings of the stepped sector type. There are several arguments which support this choice.

Because the stepped sector thrust bearing (See Figure 1 for typical configuration) is a common, popular type noted for its simplicity and relative ease of manufacture, a large volume of definitive theory and design data has been developed. The most recent and acceptable theory as yet lacks complete experimental verification. The recent development, at AiResearch, of a thrust bearing test rig capable of very high speeds affords an opportunity to obtain data in regions of operation previously unattainable. Arrangements were made for the construction of a second

Thrust Bearing Test Rig ML1606 at the Naval Postgraduate School in order to conduct this research.

2. Theoretical Considerations.

In 1886 the English scientist, Osborne Reynolds, published the defining differential equation for thick film lubrication. Several years later, Kingsbury in the United States and Michell in Australia demonstrated the applicability of the Reynolds Equation to thrust bearings by development of the tilting pad bearing. In 1918 Lord Rayleigh [1] found that for an infinitely wide, incompressible film, the optimum shape for a thrust bearing is the stepped configuration. However the step bearing can be optimized for only one expected operating speed or load but the tilting pad bearing automatically adjusts its pad angle to a new optimum as speed or load changes. Additionally, when side leakage is taken into account, the stepped bearing's load capacity markedly diminishes and its advantage over the tilting pad bearing disappears. For these reasons this bearing type was little used for liquid film lubrication. It was not until 1950 that Archibald [2] published the first analysis of a finite stepped thrust bearing using an incompressible film.

When gas is used as the lubricant, the step bearing becomes desirable for two reasons. First, for a tilting pad bearing to retain its continuous optimum operation, the position of the pad pivot point must be continually changed. This is the effect of compressibility on the bearing design. A pivot is required that consists of a cam surface that is very difficult to machine. Secondly very close machining tolerances and finishes are required on gas bearings and since the tilting pad bearing is composed of a number of close-fitting parts, it is extremely costly to produce. In comparison the step bearing is relatively cheap.

When the analysis takes into account compressible lubricants, the differential equation becomes nonlinear and several assumptions become necessary in order to obtain an analytic solution. Even though the

resulting solution is approximate it does establish a base for optimization of bearing geometry and permits correlation of theory to specific test bearings.

Figure 1 depicts the geometry of a typical stepped sector thrust pad. The upper thrust plate (plane surface) rotates with constant angular velocity ω while the lower (stepped) surface is stationary. Radial grooves of angular width δ admit gas at ambient pressure to the leading and trailing edges of each pad. The pad itself, of sector arc length γ, is divided into two sectors, one sector of length α being recessed by an amount Δ relative to the other. The larger clearance in the recessed region is designated h_1, while the smaller, or minimum, clearance is designated h_2.

In cylindrical coordinates, the compressible lubrication equations for slider bearings take the form [3]:

$$\frac{\partial p}{\partial r} = \mu \frac{\partial^2 V_r}{\partial z^2} \tag{1}$$

$$\frac{1}{r}\frac{\partial p}{\partial r} = \mu \frac{\partial^2 V_\theta}{\partial z^2} \tag{2}$$

$$\frac{\rho V_r}{r} + \frac{\partial}{\partial r}(\rho V_r) + \frac{1}{r}\frac{\partial}{\partial \theta}(\rho V_\theta) = 0 \tag{3}$$

$$\frac{Q_r}{r} + \frac{\partial Q_r}{\partial r} + \frac{1}{r}\frac{\partial Q_\theta}{\partial \theta} = 0 \tag{3a}$$

$$\frac{\rho}{\rho_a} = \frac{p}{p_a} \tag{4}$$

where V_r and V_θ are the radial and tangential components of lubricant velocity, Q_r is the radial mass flow rate per unit circumferential width and Q_θ is the circumferential mass flow rate per unit radial width.

To obtain these equations, the following assumptions were made: (a) the flow is steady (does not vary with time); (b) the film thickness is at least two orders of magnitude smaller than r or $r\Theta$; (c) the axial, z, component of velocity and its derivatives are negligibly small; and (d) the gas lubricant behaves as a perfect gas and compresses and expands isothermally within the bearing.

By introducing the boundary conditions:

$$V_r(z=0) = 0$$

$$V_r(z=h) = 0$$

$$V_\theta(z=0) = r\omega$$

$$V_\theta(z=h) = 0$$

and integrating equations (1) and (2) the following expressions for the mass flow rates can be obtained:

$$Q_r = -\frac{\rho h^3}{12\mu}\cdot\frac{\partial p}{\partial r} \tag{5}$$

$$Q_\theta = r\left[\frac{\rho\omega h}{2} - \frac{\rho h^3}{12\mu r^2}\cdot\frac{\partial p}{\partial\theta}\right] \tag{6}$$

Ausman [4] introduced equation (4) and made the assumptions that (a) ρ_a may be substituted for ρ , ignoring the effect of compressibility on the pressure gradient terms and (b) r^{-2} in equation (6) may be replaced with r_1^{-2} where r_1 is some constant such that $bR < r_1 < R$ where b is the ratio of inner to outer bearing radii = r_i /R. The first assumption linearizes the resulting differential equation while the second makes the variables separable. Further, introduction of two dimensionless variables,

$$\bar{p} = \frac{p - p_a}{p_a}$$

$$\bar{r} = \frac{r}{R}$$

and substitution of equations (5) and (6) into equation (3a) results in the linearized, separable differential equation

$$\frac{\partial^2 \bar{P}}{\partial \bar{r}^2} + \frac{1}{\bar{r}} \cdot \frac{\partial \bar{P}}{\partial \bar{r}} + \left(\frac{R}{r_1}\right)^2 \frac{\partial^2 \bar{P}}{\partial \theta^2} = \Lambda \frac{\partial \bar{P}}{\partial \theta} \tag{7}$$

where

$$\Lambda = \frac{6 \mu \omega R^2}{p_a h^2} \tag{8}$$

Equation (8) defines the dimensionless parameter known as bearing number, Λ . The form of the solution is

$$\bar{P} = X(\bar{r}) \cdot Y(\theta) \tag{9}$$

and results in an infinite series solution which must be solved independently for each flow region.

Boundary conditions state that the pressure equals the ambient pressure at both inside and outside bearing radii, and that the pressure and flow rate are equal at the step when approached from either direction. These latter conditions are met by an iterative process which seeks a value for r_1 which, when substituted into the two series solutions, results in equal solutions at the step for both regions.

The theoretical load carrying capacity for a bearing is found by integrating the expression for $\bar{p}$ over the bearing area.

Ausman then optimized bearing geometry by independently varying step location, τ/γ , and number of pads, n, and solving for these parameters at maximum load capacity. He presented his results in the form of one table and one graph from which a designer can determine the complete optimum geometry for a given bearing size and expected operating point (bearing number, Λ). In his optimization he assumed that the

optimum compression ratio, q, was 2.0 where $q = h_1/h_2 = (h_2 + \Delta)/h_2$ $= 1 + 1/\alpha$. This, he found from trial solutions, was a good assumption over a wide range of bearing numbers. Note in Figure 3 (which is described later) that the solution for constant minimum clearance is maximum at a clearance ratio of 1.0 which corresponds to q = 2.0.

Wildmann, et. al., in a comprehensive study [5], obtained extensive experimental data at low bearing numbers which essentially confirmed Ausman's theory in the regions the study undertook to investigate. Ausman's results were significantly simplified by the introduction of a modified bearing number

$$\Lambda' = \frac{6\mu\omega R^2}{p_a h_2^2}(1-b^2) = \Lambda(1-b^2) \qquad (10)$$

This enabled him to eliminate the radius ratio, b, as an independent parameter and to present load capacity for optimum compression ratio (q = 2) as one curve plotted against bearing number. This curve is shown as Figure 2.

As a result of experimental data, slight modifications were made to Ausman's theoretical design parameters. New design parameters were presented in graphical form so that design of a specific bearing could be undertaken without the necessity of extrapolating Ausman's tabular results. The first two design charts are similar to Figures 2 and 3 but reflect Wildmann's correlation of theory. The remaining three are plots of optimum sector ratio, $\eta = \tau/\gamma$, and optimum sector arc length (degrees) and optimum number of sectors, n, all plotted vs. modified bearing number. The test bearing investigated in this study is designed using the parameters given by Wildmann.

One additional curve, computed from Ausman's theory and presented in Wildmann's study, is shown as Figure 3 because of its usefulness in comparing experimental results with theory. This consists of a plot of minimum clearance ratio, h_2 / Δ , vs.

$$\text{Load Ratio} = \frac{\text{Load}}{\text{Optimized Load for } q = 2}$$

for a constant step depth, Δ .

3. Description of Apparatus

Trust Bearing Test Rig

The primary research tool used in this experimental investigation is the AiResearch Thrust Bearing Test Rig, ML 1606, an extremely versatile device designed to measure the operating characteristics of gas lubricated thrust bearings at very high rotation rates. Rotating speed and bearing load can be continuously varied and accurately measured while instrumentation can be provided for measurement of air film thickness, torque, and temperatures at selected points. Design variations permit testing thrust bearings up to six inches in diameter and test bearings may be of any type or configuration.

Photographs of the Thrust Bearing Test Rig and its associated instrumentation are shown in Figures 4 and 5. A schematic of the arrangement of major components is presented in Figure 6. The rotating assembly consists of a hardened stainless steel shaft one inch in diameter with an integral 2½ inch diameter thrust disc on the lower end and a small air driven turbine wheel on the upper end. This shaft is supported vertically in two AiResearch ARPF compliant journal bearings. It is supported from beneath by the test bearing and separation of the back of the thrust plate from the upper body of the machine is maintained by an externally pressurized air thrust bearing. This configuration is capable of rotation rates up to 105,000 RPM after running through the half-frequency whirl region encountered in the range between 20,000 and 50,000 RPM.

The test bearing is supported beneath the thrust runner on the top face of a heavy steel piston which moves vertically and through a small rotation angle within a cylinder equipped with a hydrostatic air bearing.

In the tests performed the test bearing was recessed into the face

of the piston and was gimballed by placing it on a 3/32 inch thick sheet of gasket rubber. Restraint in torque was provided by securing a .020 inch x ½ inch piece of piano wire in a groove on the piston face in such a way as to allow the end of the wire to extend into the bottom of one of the air inlet grooves on the test bearing. A photograph of the bearing secured in place is shown as Figure 7.

Air Supply and Control System

A schematic of the air supply system is shown in Figure 8. The system utilizes a 50 HP Westinghouse 220 VAC, 3 phase, 60 hertz, Induction Motor to drive a Chicago Pneumatic, Model P2CB Two Stage Air Compressor with intercooler (max pressure = 450 psi). The output air is cooled by a Heliflow shell and tube heat exchanger, Type 9AA14S. Water and oil are removed by a Wright-Austin Co., separator and float trap. These are followed by a Morse Diving Equipment Co., air filter and a standpipe containing a dessicant to further dry the air. Airflow to the receivers is controlled by a Bailey Indicator Controller, Type K47, actuating a Bailey Diaphram Valve Type ½ XSDS-9M. The compressed air is stored in two American Pipe & Steel Corp., Vertical Air Receivers (each with a volume of 117 ft^3. , max. pressure = 500 psi). Air is drawn from the top of both receivers and is distributed at outlets in a small manifold near the test setup.

Figure 9 depicts schematically the air supply and flow control arrangement to the test rig itself. Figures 4 and 5 are photographs of the actual apparatus. Air is provided to the driving turbine through a one inch line fitted with a regulator and globe valve for rough speed control. Fine control is achieved by a ½ in. line equipped with a regulator and needle valve. This line is placed in parallel around the rough control

line. A ½ in. line with a secondary filter and needle valve provides 120 psig air to the hydrostatic thrust bearing. Air is supplied to the hydrostatic piston journal bearing at 20 psig by a ½ in. line with regulator and needle valve. A similar arrangement provides air to load the piston from beneath, however an atmospheric bleed is placed in this line to prevent pressure buildup due to low flow rates. Bourdon type pressure gages are located as shown in the schematic. Loading piston pressure is measured by a 14 inch mercury U-tube manometer.

Electronic Instrumentation

Figure 10 schematically describes the electronic instrumentation used to measure rotational speed, air film thickness and temperature.

Rotational speed of the test rig shaft is sensed by a Pace Engineering Co. SU-2 Pickup which is a very sensitive coil with a core of flexible iron straps. The coil, when placed in the vicinity of a rotating shaft of ferromagnetic material, generates a small A.C. voltage of varying frequency as a result of the rotating magnetic field due to residual permanent magnetism in the shaft. The Pace Pickup was placed as shown in Figure 4 and its output was displayed on the y-axis of a Hewlett-Packard Model 130C Oscilloscope and a Hewlett-Packard Electronic Frequency Meter Model 500A. The output of a Donner Sine Wave Generator Model 1202 was displayed on the X-axis of the oscilloscope and its frequency was accurately measured by a Systron-Donner Digital Counter Model 1013D. Since rotation rate is a predetermined figure for each data run, the rate is preset on the sine wave generator and the speed of the rig is adjusted until a stationary elliptical lisajous figure is achieved on the cathode ray tube, indicating that the two frequencies are matched. This results in a speed measurement accurate to plus or minus one hertz or $\pm$ 0.1% at 60,000 RPM.

Air film thickness measurements were made using Bently Proximitor distance detectors. The calibration and accuracy determination of this system is presented in Appendix A. During initial runs to check out the equipment it was found that heating and cooling of the distance probe (located in the center of the test bearing) was more extensive and more rapid than anticipated. This change in temperature causes a resistance change in the sensing coil and hence changes the output voltage for a given distance. Further, due to low friction, rundown time (time necessary to stop the shaft) was in excess of one minute and during this time the temperature and therefore the probe zero reading (thrust runner and bearing in contact), changed markedly. To correct this, two steps were taken.

Two air nozzles made of ¼ inch copper tubing were secured in the turbine outlet throat to direct air jets against the turbine blades opposite to the direction of rotation. To actuate these, two spring loaded, quick acting valves were installed. This system, seen in Figure 4 stopped the shaft in an average time of 15 seconds.

Two copper-constantan thermocouples were installed, one adjacent to the distance probe face and touching it, and the other in an ice-water bath as a reference junction. The output was recorded on a Mosely Autograf Strip Chart Recorder Model 7100B. The second channel of the recorder was used as an event marker to record points at which data was taken. This arrangement is shown in Figure 10.

These two corrective measures enabled the author to establish the probe temperature difference between the probe reading and the zero reading (thrust runner and bearing in contact) for each data point. The significance of this data will be shown in Appendix C - Experimental Uncertainty Intervals.

Test Bearings

It was originally intended to test several thrust bearings of different optimum configurations but time and funding limitations restricted the tests to one bearing. The bearing was chosen to correspond to the point in Ausman's Table I [4] at b = .20, $\Lambda = \Lambda_\Delta = 160$. The design parameters however, were taken from Wildmann [5]. These parameters are:

$$b = .20$$

$$\Lambda'_\Delta = \Lambda_\Delta (1 - b^2) = 153.7$$

$$\eta = \tau/\gamma = .135$$

$$n = 3$$

$$\gamma = 118°$$

$$\tau = 16°$$

The minimum film thickness was chosen to be 250. microinches so, for q = 2.0, the optimum step depth, Δ , is 250. microinches. The outside radius, R, was chosen as 1.125 inches. The final design based on these parameters is shown in Figure 11. Note the air inlet groove which is two degrees wide at the average radius. The material chosen for the bearing was "Graphmo" tool steel, a graphite-molybdenum steel noted for its wear resistance and low sliding friction. The bearing was manufactured to specifications by B & W Precision, Inc., Glendale, California.

Inspection of the bearing by optical flat before running revealed a flatness of $\pm$ 5.0 microinches across the bearing face. Profilometer readings by the manufacturer showed a surface roughness of 5 microinches (rms). The step depth was measured on a Johansson Mikrokator Comparator and varied between 230 and 270 microinches with an average of 250. These readings were taken numerous times across all three steps. The surface of the recessed area was somewhat rougher than the raised portion but was not measured.

4. Experimental Procedure

Data was obtained in such a manner that load vs. air film thickness could be plotted for a single constant speed. This was repeated for a number of different speeds to obtain a family of such curves. No data was taken in the region where half-frequency whirl was encountered to insure that the data was not affected by this instability.

Test Rig Operation

All runs were made with the hydrostatic thrust air set at 115 to 120 psig and the hydrostatic piston journal air adjusted to 20 psig. All starts and stops were performed with a test bearing load of 3.65 pounds (3.0 inches Hg). Prior to starting, the speed for the run (revolutions per second) was preset on the digital counter by adjusting the sine wave generator to the same frequency (hertz). The turbine was then started by quickly opening the rough control valve enough to bring the downstream pressure to about 5 psig. The bearing noise was monitored continuously for whirl or rubbing by listening with an automotive type stethoscope. Rotational speed was adjusted while watching the lisajous figure on the oscilloscope and reading the frequency meter until the speed was slightly greater than the preset rate and steady. The temperature recorder chart was then started and the bearing load slowly increased, taking care that the temperature did not increase at a rapid rate and cause excessive thermal distortion. As the bearing was loaded, the turbine air flow was increased to maintain speed.

When the load for the particular data point was reached, the rig was allowed to run until the temperature reached a steady state or was increasing very slowly. Then the fine speed control flow valve was used to control turbine speed until the oscilloscope trace showed an exact frequency match. At this point, the distance probe output was read and

noted, the turbine air was secured, the braking jets were actuated, and the bearing load was reduced to 3.65 pounds. As the probe output was read, the event was marked on the strip chart recorder. At the instant that the shaft stopped and the thrust disc and bearing came in contact, the distance probe output was again read and the event marked.

This procedure was repeated for each data point obtained, and each data point was repeated several times to insure correctness and to obtain a statistical average. The data obtained are presented in Tables 1 through 4.

Bearing Failure

On the last run for data, a failure occurred and the thrust plate contacted the bearing face with subsequent rapid loss of air film and wiping of the bearing surfaces. The failure was initiated at a speed of 72,000 RPM and a bearing load of 14.7 pounds. Just prior to failure a vibration noise began and increased in amplitude even though the load was reduced sharply. The center of both the bearing and thrust disc were wiped to a radius of approximately .35 inches which would seem to indicate failure due to thermal distortion. This is felt not to be the case, however, since neither temperature nor temperature rate were excessive at the time, and the load, while high, was no higher than for several other runs when the air film thickness was even less. Rather it is felt that the speed used was a critical vibration frequency for some component, most likely the rubber sheet used to gimbal the test bearing. The appearance of the surfaces after failure merely indicates that slight thermal distortion was present at the time of failure.

Data Reduction Calculations

The data reduction calculations used to obtain the results presented in the next section are described in Appendix B.

5. Results

The numerical results calculated from the data obtained are presented in Table 5.

Figures 12 through 15 are plots of bearing load vs. air film thickness for each speed tested. All data points are plotted and extreme uncertainty limits are shown. Figure 16 is a composite plot of the same data using only the statistical averages for air film thickness.

Figure 17 is a graph of dimensionless load parameter, L, vs. the modified bearing number, Λ'_{ij}, for a compression ratio, q = 2.0.

Perhaps the most useful form of presenting the results is seen in Figure 18. The ratio of actual load to optimized load at q = 2.0 is shown on the ordinate logarithmically while the clearance ratio, $\propto = h_2/\Delta$ is plotted on the abcissa. By the optimized load it is meant the optimized load from the theoretical curve in Figure 2 determined for the same bearing number as the particular data point under consideration. A clearance ratio of 1.0 corresponds to q = 2.0. All of the data points from Figure 17 are shown in Figure 19.

6. Comparison of Results with Theory

In Figure 19, the results shown in Figure 17 are superimposed on a reproduction of Wildmann's Design Chart A [5], which predicts load carrying capacity at q = 2.0 for a given bearing number, Λ' . Note that the results take roughly the same form as the predicted curve but the load capacity is signifigantly lower.

In Figure 20, the curve from Figure 18 is replotted on a graph which shows both Ausman's theoretical prediction and Wildmann's experimental results. Note that the results of this study have not been normalized to a load ratio of 1.0 as was done in the study compiled by Wildmann.

Two factors are immediately apparent. The first is that the slope of the curve obtained in the current study is essentially the same as Wildmann's correlation curve. Secondly, the new curve predicts a load capacity that is a constant fraction, 2/5 or 0.4 of that predicted by the design curves [5] based on Ausman's work.

7. Discussion of Results

It is felt that the careful calibration of the probes used to measure air film thickness, plus the temperature monitoring employed, resulted in reliable air film thickness measurements. Further, the repetition of data points and use of average values reduced random error. This opinion is borne out by the smoothness of the load vs. film thickness curves and the consistency of the load ratio vs. clearance ratio curve.

There are two sources of possible major error. The first is due to the near impossibility of constructing the perfect stepped sector thrust bearing upon which the theory is based. It was noted that the variation in the step depth was plus and minus 20 microinches or 12% of the specified depth. This plus the rougher finish on the recessed area undoubtedly affected the flow characteristics of the lubricant. The second serious condition is thermal distortion. Even though attempts were made to allow temperature to reach a steady state, distortion was surely present as shown by the nature of the bearing failure which occurred. Thermal distortion would result in a nonuniform air film thickness; the film would increase in thickness as the radius at which it is measured is increased. It is not felt, however, that either of these conditions are responsible for the wide disparity between theory and experiment with regard to load capacity, particularly since the data is otherwise consistent.

8. Conclusions

From the comparison of results with theory, it is concluded that: (a) Wildmann's correlation of the variation of load ratio with clearance ratio is correct at high bearing numbers for the bearing tested; (b) Ausman's theory correctly predicts the shape of the load vs. bearing number curve in the high bearing number region, and (c) the prediction of the magnitude of the load capacity is in error in this region.

Ausman, in the preparation of his design table, performed separate optimizations for bearing geometry but extrapolated load capacity from curves computed for a central point in the table. He warned his readers that the accuracy of this extrapolation probably decreased with distance from the center of the table. The results of this test, of a bearing purposely chosen from an extreme corner of his table, confirm that Ausman's intuition was correct.

9. Recommendations for Further Study

Now that it is established that there is a limit to the range of accuracy of Ausman's design parameters, additional bearings, optimized by the procedure used in this study, should be tested until the range of accuracy is established.

A computer aided analysis of the load capacity equations should be performed over the full range of bearing numbers using the modified bearing number introduced by Wildmann. The results should give some insight into the true nature of the relationship and could result in a revision of the optimized design parameters.

Other types of thrust bearings, such as the spiral groove or herringbone patterns, await testing at high bearing numbers. The AiResearch Thrust Bearing Test Rig is ideal for this purpose.

REFERENCES

[1] Rayleigh, Lord, "Notes on the Theory of Lubrication," Phil. Mag., 35, 1-12, 1918.

[2] Archibald, F. R., "A Simple Hydrodynamic Thrust Bearing," Trans. ASME, 72, 393-400, 1950.

[3] Mow, C. C. and Saibel, E., "The Gas Lubricated Sector Thrust Bearing," ASME Paper 58-Lub-5.

[4] Ausman, J. S., "An Approximate Analytical Solution for Self-Acting Gas Lubrication of Stepped Sector Thrust Bearings," ASME Trans., 4, 304-314, 1961.

[5] Wildmann, M., et. al., "Gas Lubricated Stepped Thrust Bearing -- A Comprehensive Study," ASME Jour. of Basic Eng., March 1965, 213-229.

[6] Kochi, K. C., "Characteristics of a Self-Lubricated Stepped Thrust Pad of Infinite Width with Compressible Lubricant," Trans. ASME, 81, 135-146, 1959.

[7] Gross, W. A., Gas Film Lubrication, John Wiley and Sons, Inc., New York, 1962.

[8] Grassam, N. S. and Powell, J. W., Editors, Gas Lubricated Bearings, Butterworths, London, 1964.

[9] Kline, S. J. and McClintock, F. A., "Describing Uncertainties in Single-Sample Experiments," Mech. Eng., Jan. 1953, 3-8.

TABLE 1

Summary of Data -- 54,000 RPM

RUN NO.	LOAD (pounds)	h_2 (μ in.)
14-1	6.59	363
14-2	6.59	366
14-3	6.59	371
14-4	6.59	363
14-5	6.59	366
14-6	6.59	370
15-1	8.62	318
15-2	8.62	330
15-3	8.62	337
15-4	8.62	320
15-5	8.62	325
15-6	8.62	320
16-1	10.65	287
16-2	10.65	287
16-3	10.65	287
16-4	10.65	284
16-5	10.65	289
16-6	10.65	294
17-1	12.67	254
17-2	12.67	260
17-3	12.67	256
17-4	12.67	258
17-5	12.67	254
17-6	12.67	253

TABLE 1 (Cont)

RUN NO.	LOAD (pounds)	h_2 ($\frac{1}{4}$ in.)
18-1	13.69	246
18-2	13.69	246
18-3	13.69	244
18-4	13.69	251
18-5	13.69	243
18-6	13.69	250

TABLE 2

Summary of Data -- 60,000 RPM

RUN NO.	LOAD (pounds)	h_2 (μ in.)
1-1	no data	
2-1	4.06	442
2-2	4.06	452
2-3	4.06	455
2-4	4.06	466
2-5	4.06	456
2-6	4.06	455
3-1	6.59	360
3-2	6.59	363
3-3	6.59	370
3-4	6.59	380
3-5	6.59	385
3-6	6.59	394
4-1	8.62	320
4-2	8.62	313
4-3	8.62	330
4-4	8.62	333
4-5	8.62	337
4-6	8.62	328
5-1	10.65	298
5-2	10.65	294
5-3	10.65	294
5-4	10.65	296
5-5	10.65	299

TABLE 2 (Cont)

RUN NO.	LOAD (pounds)	h_2 (4 in.)
5-6	10.65	289
6-1	12.67	256
6-2	12.67	257
6-3	12.67	256
6-4	12.67	268
6-5	12.67	261
6-6	12.67	260
7-1	13.69	243
7-2	13.69	251
7-3	13.69	253
7-4	no data	
7-5	13.69	253
7-6	13.69	251
7-7	13.69	253
8-1	14.19	240
8-2	14.19	250
8-3	14.19	241
8-4	14.19	240
8-5	14.19	243
8-6	14.19	240

TABLE 3

Summary of Data -- 66,420 RPM

RUN NO.	LOAD (pounds)	h_2 (μ in.)
9-1	6.59	376
9-2	6.59	380
9-3	6.59	385
9-4	6.59	385
9-5	6.59	377
9-6	6.59	374
10-1	8.62	332
10-2	8.62	347
10-3	8.62	337
10-4	8.62	339
10-5	8.62	336
10-6	8.62	337
11-1	10.65	299
11-2	10.65	305
11-3	10.65	312
11-4	10.65	295
11-5	10.65	295
11-6	10.65	298
12-1	12.67	263
12-2	12.67	274
12-3	12.67	264
12-4	12.67	274
12-5	12.67	268

TABLE 3 (Cont)

RUN NO.	LOAD (pounds)	h_2 (μin.)
13-1	14.70	250
13-2	14.70	247
13-3	14.70	240
13-4	14.70	247
13-5	14.70	243
13-6	14.70	246

TABLE 4

Summary of Data -- 72,000 RPM

RUN NO.	LOAD (pounds)	h_2 (μ in.)
19-1	8.62	337
19-2	8.62	353
19-3	8.62	346
20-1	10.65	301
20-2	10.65	301
20-3	10.65	301
21-1	12.67	265
21-2	12.67	267
21-3	12.67	277
22-1	13.69	258
22-2	13.69	260
23-1	14.70	253
23-2	14.70	Bearing failure.

TABLE 5

Tabulation of Results

Run No.	Speed (rpm)	Load (lbf.)	Avg. h_2 (μin.)	Bearing No. (Λ'_Δ)	L	L_{OPT}	L/L_{OPT}	h_2/Δ
14	54,000	6.59	366.5	123.0	.1193	.598	.199	1.47
15	54,000	8.62	325.0	123.0	.1561	.598	.261	1.30
16	54,000	10.65	288.0	123.0	.1929	.598	.323	1.15
17	54,000	12.67	255.8	123.0	.2295	.598	.384	1.02
18	54,000	13.69	246.7	123.0	.2480	.598	.415	.987
2	60,000	4.06	454.3	138.5	.0735	.628	.117	1.82
3	60,000	6.59	375.3	138.5	.1193	.628	.190	1.50
4	60,000	8.62	326.8	137.7	.1561	.627	.249	1.31
5	60,000	10.65	295.0	137.7	.1929	.627	.308	1.18
6	60,000	12.67	259.7	137.7	.2295	.627	.366	1.04
7	60,000	13.69	252.2	137.7	.2480	.627	.396	1.01
8	60,000	14.19	242.3	137.7	.2570	.627	.410	.969
9	66,420	6.59	379.5	152.1	.1193	.654	.182	1.52
10	66,420	8.62	338.0	152.1	.1561	.654	.239	1.35
11	66,420	10.65	300.7	152.1	.1929	.654	.295	1.20
12	66,420	12.67	270.0	152.1	.2295	.654	.351	1.08

TABLE 5 (Cont)

Run No.	Speed (rpm)	Load (lbf.)	Avg. h_2 (μ in.)	Bearing No. (Λ'_Δ)	L	L_{OPT}	L/L_{OPT}	h_2/Δ
13	66,420	14.70	245.5	152.1	.2663	.654	.407	.982
19	72,000	8.62	345.3	165.4	.1561	.672	.232	1.38
20	72,000	10.65	301.0	165.4	.1929	.672	.287	1.20
21	72,000	12.67	269.7	165.4	.2295	.672	.342	1.08
22	72,000	13.69	259.0	165.4	.2480	.672	.369	1.04
23	72,000	14.70	253.0	165.4	.2663	.672	.396	1.01

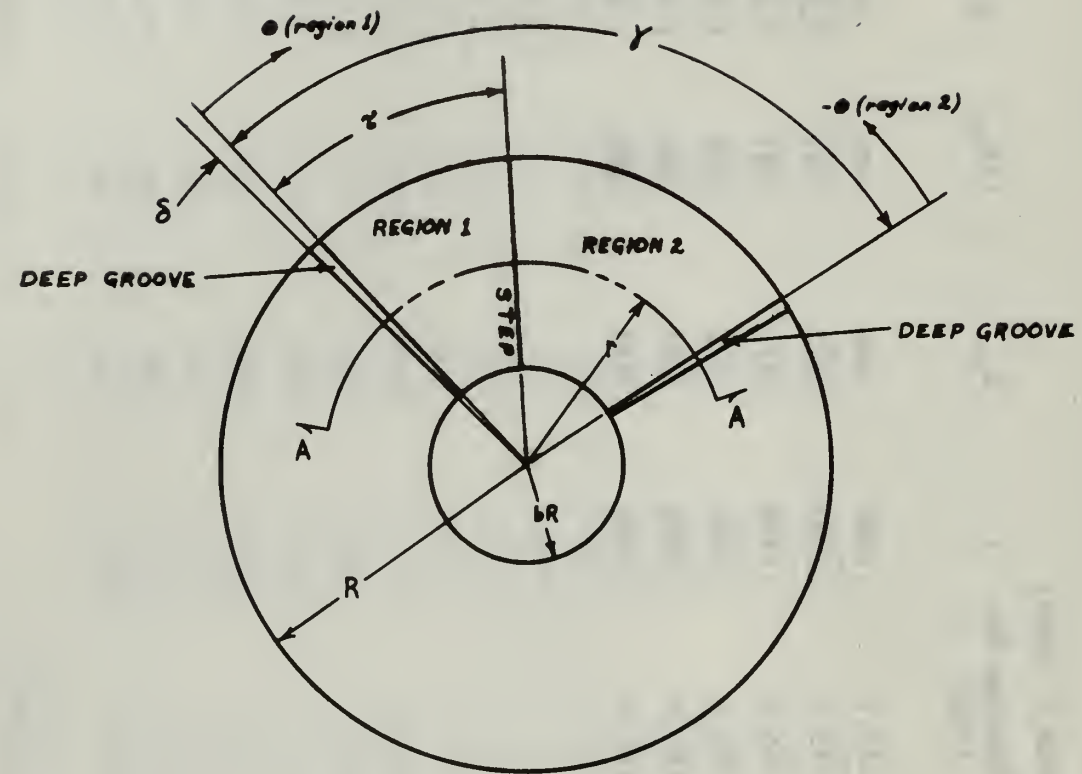

SECTION A–A

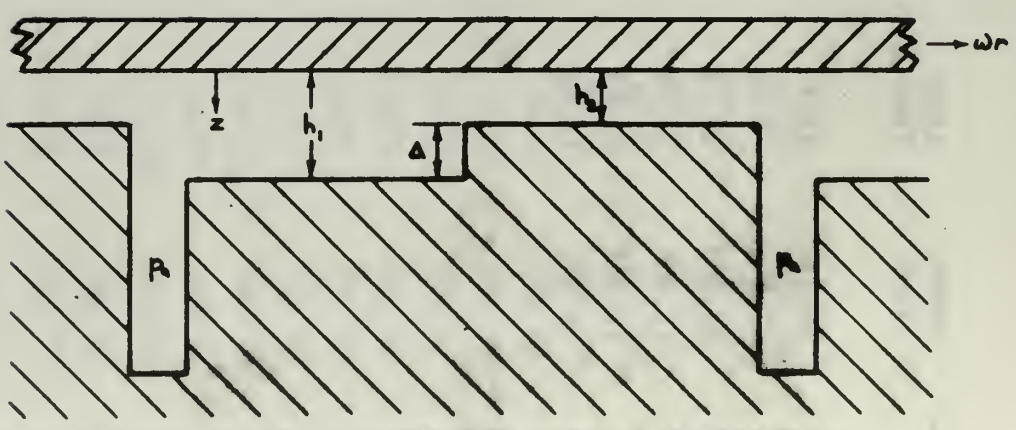

NOT SHOWN TO SCALE -- CLEARANCES GREATLY EXAGGERATED

FIGURE 1. TYPICAL STEP BEARING GEOMETRY

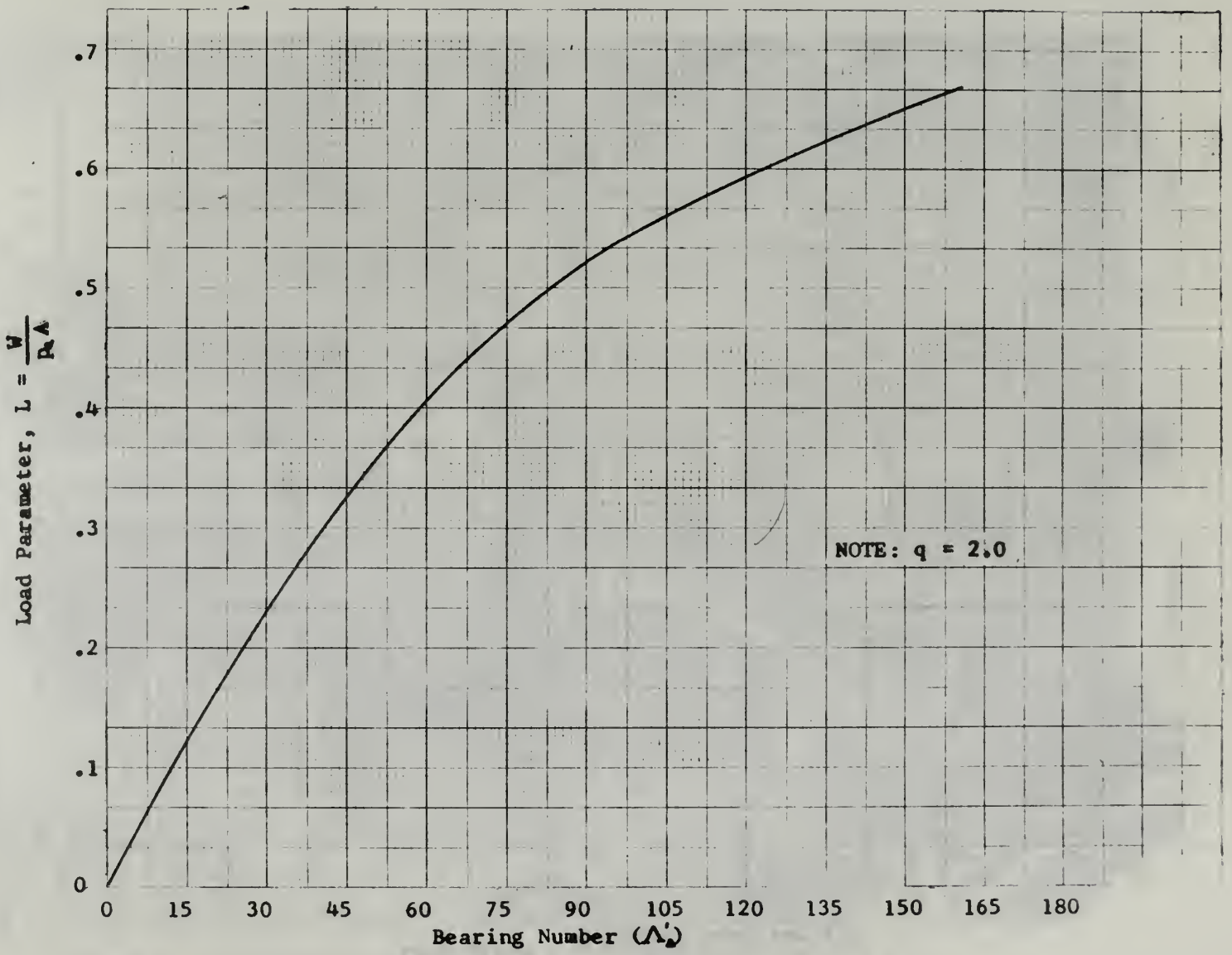

FIGURE 2. THEORETICAL LOAD CAPACITY FOR COMPRESSION RATIO = 2.0

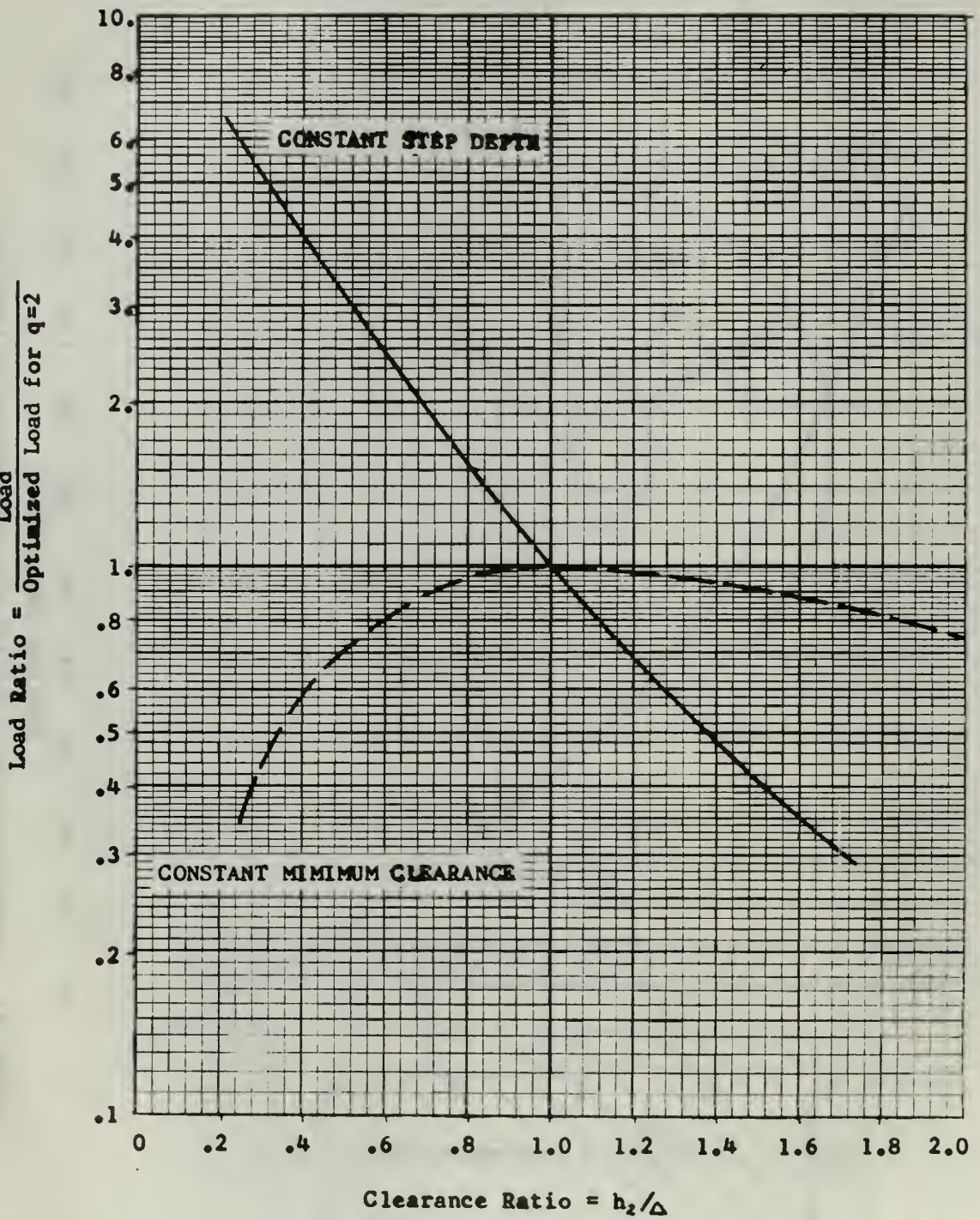

FIGURE 3. THEORETICAL VARIATION IN LOAD RATIO AS A FUNCTION OF CLEARANCE RATIO DETERMINED FOR $\Lambda = 30$

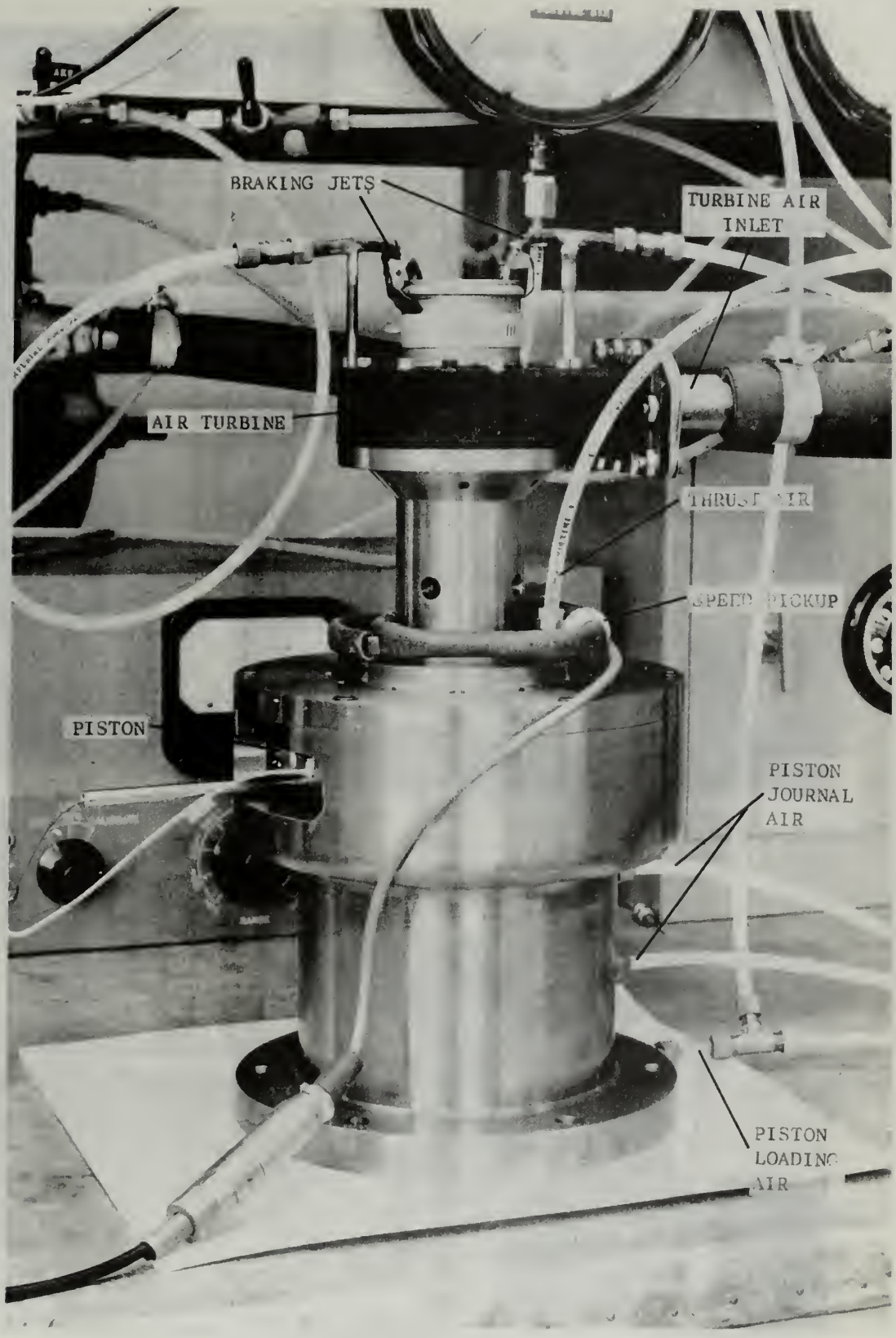

FIGURE 4. AIRESEARCH THRUST BEARING TEST RIG, ML1606

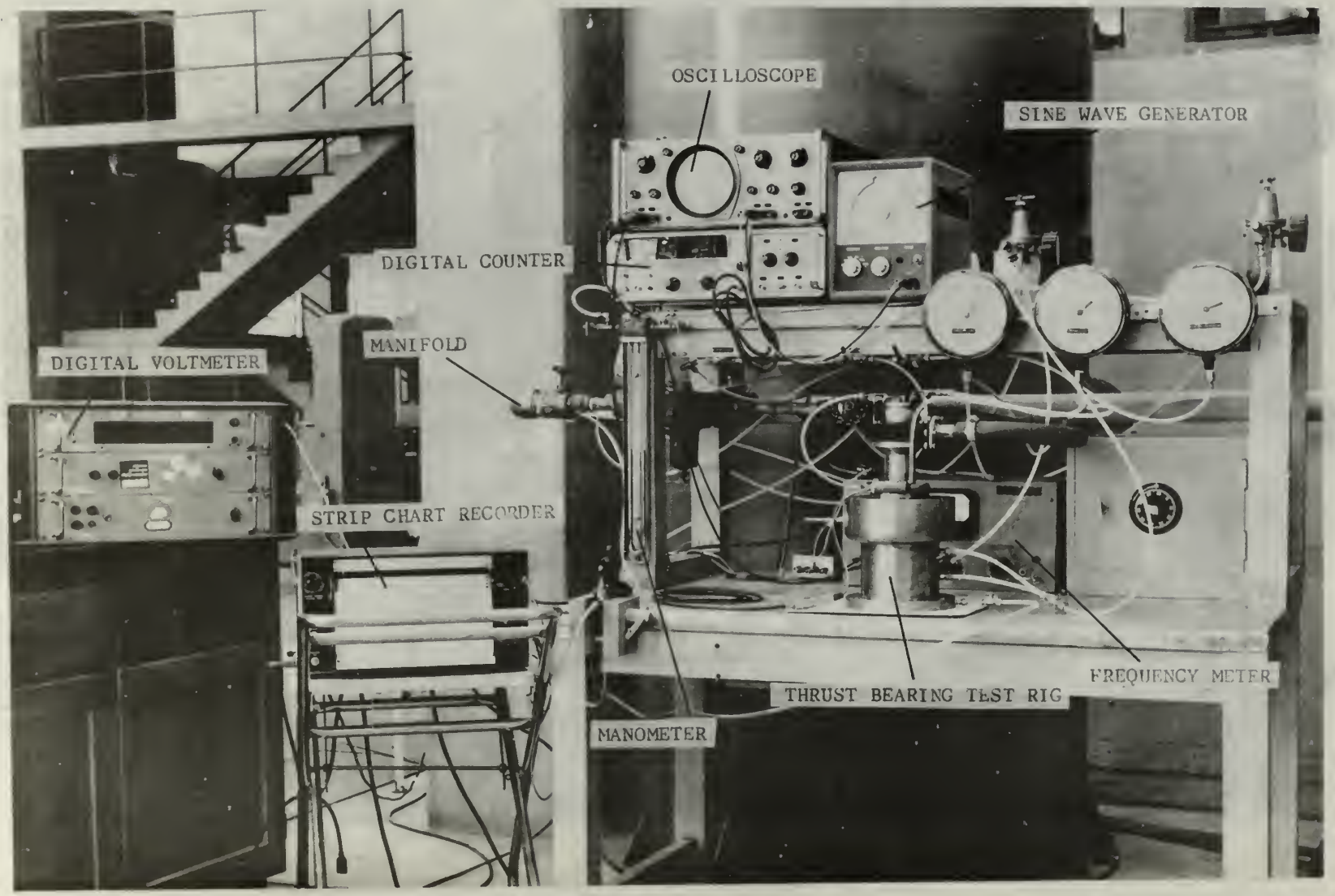

FIGURE 5. OVERALL VIEW OF TEST APPARATUS

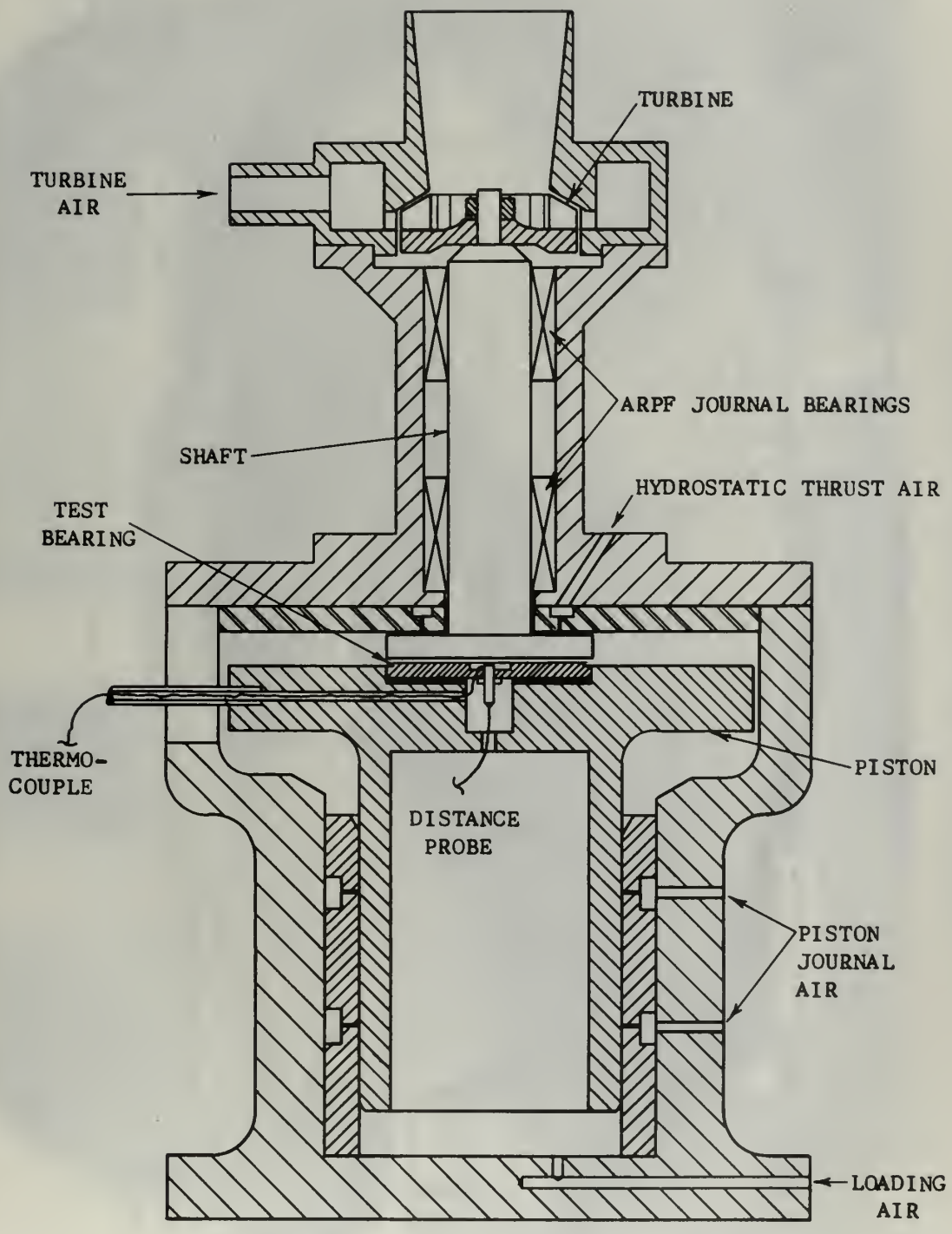

FIGURE 6. MAJOR COMPONENTS OF THRUST BEARING TEST RIG

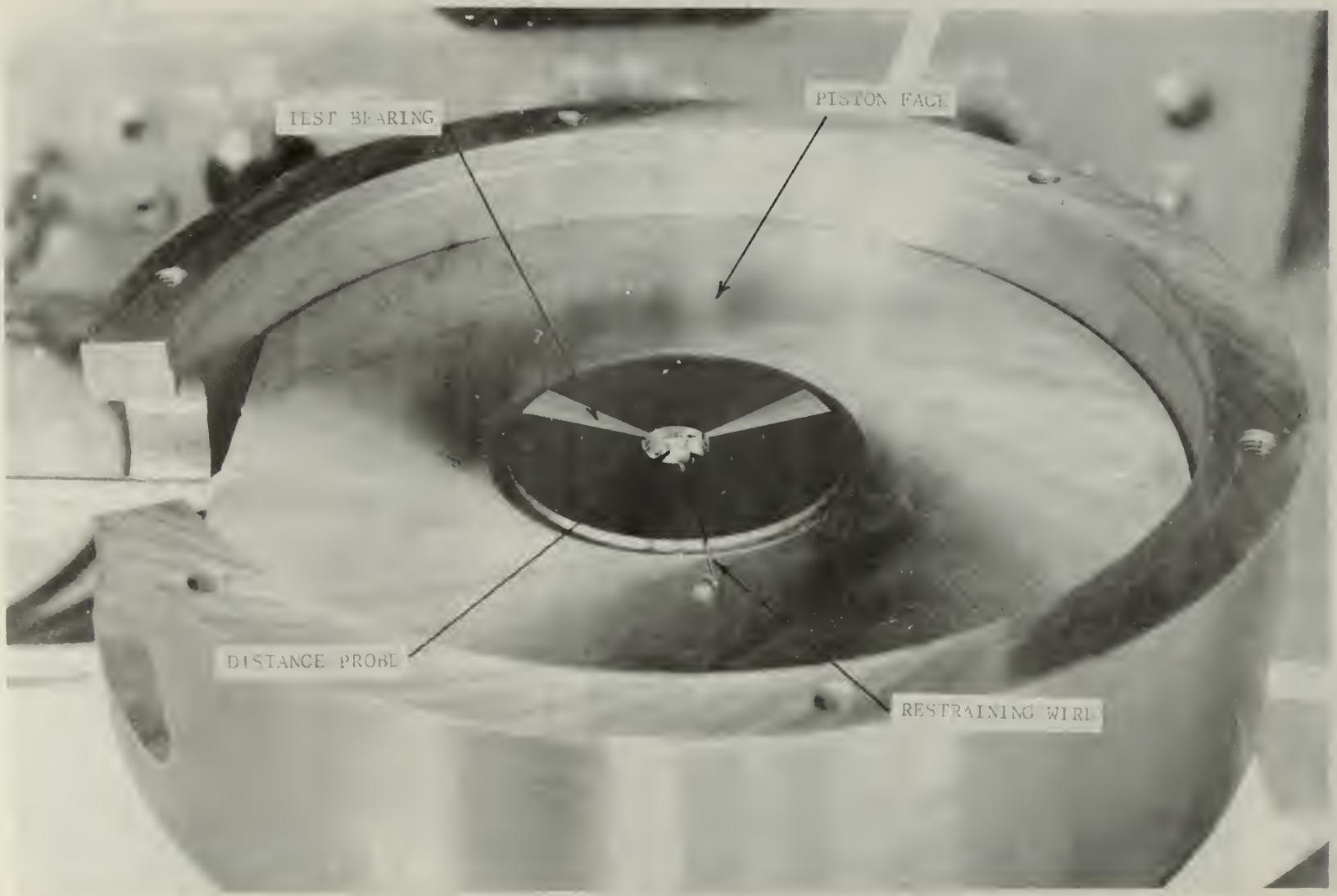

FIGURE 7. TEST BEARING IN PLACE ON PISTON FACE

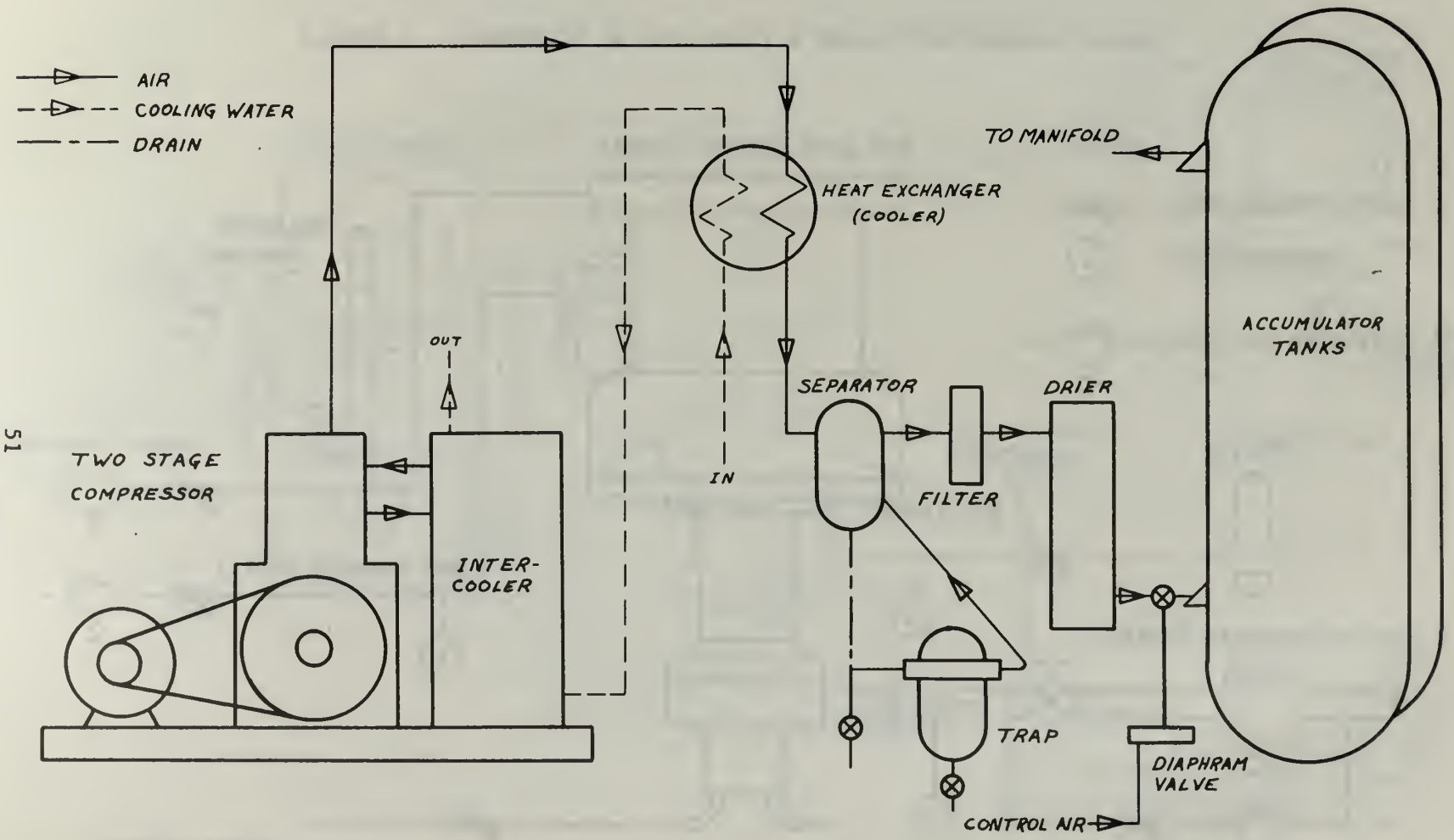

FIGURE 8. SCHEMATIC OF AIR SUPPLY SYSTEM

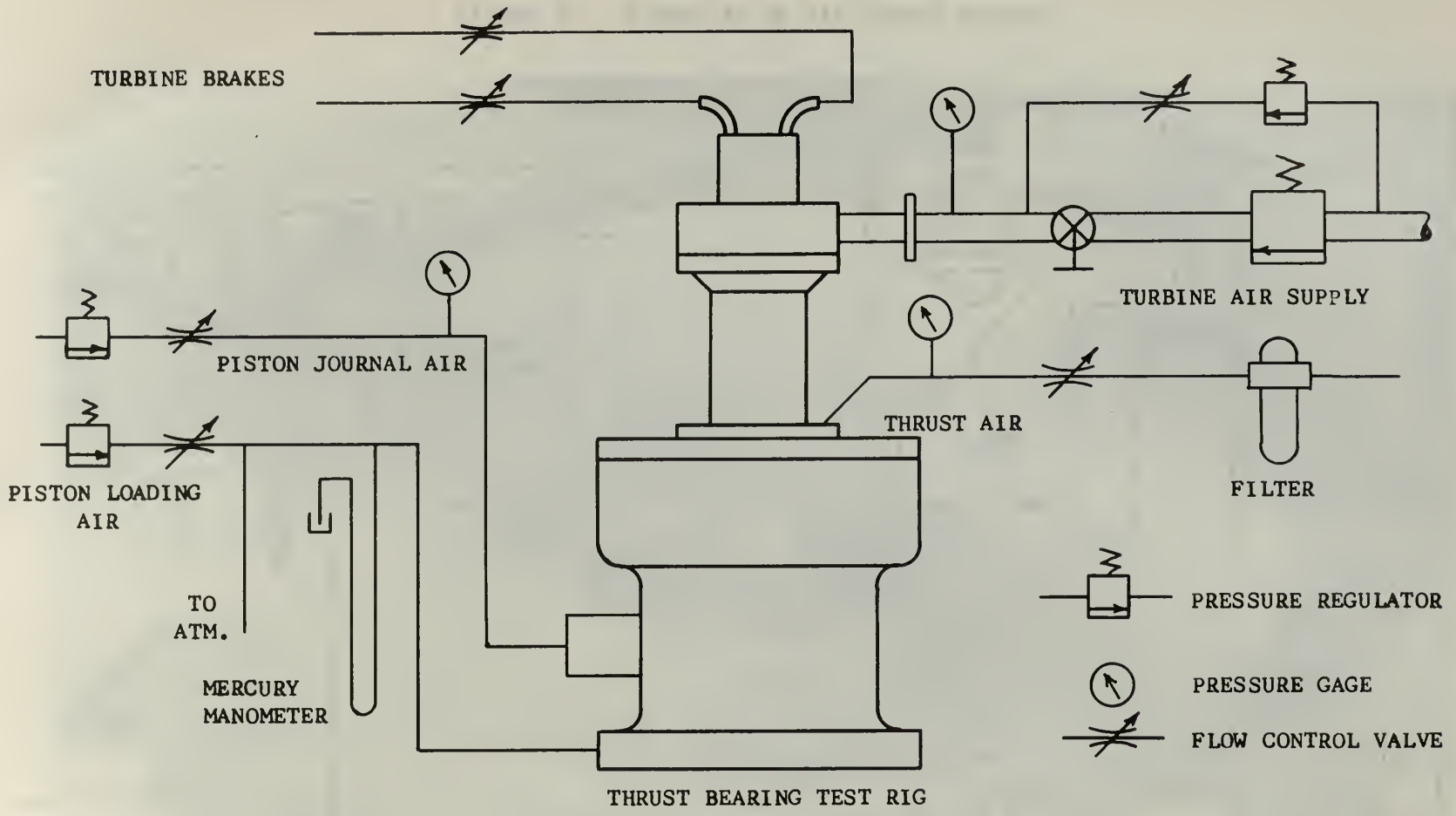

FIGURE 9. SCHEMATIC OF TEST RIG AIR SUPPLY AND CONTROL SYSTEM

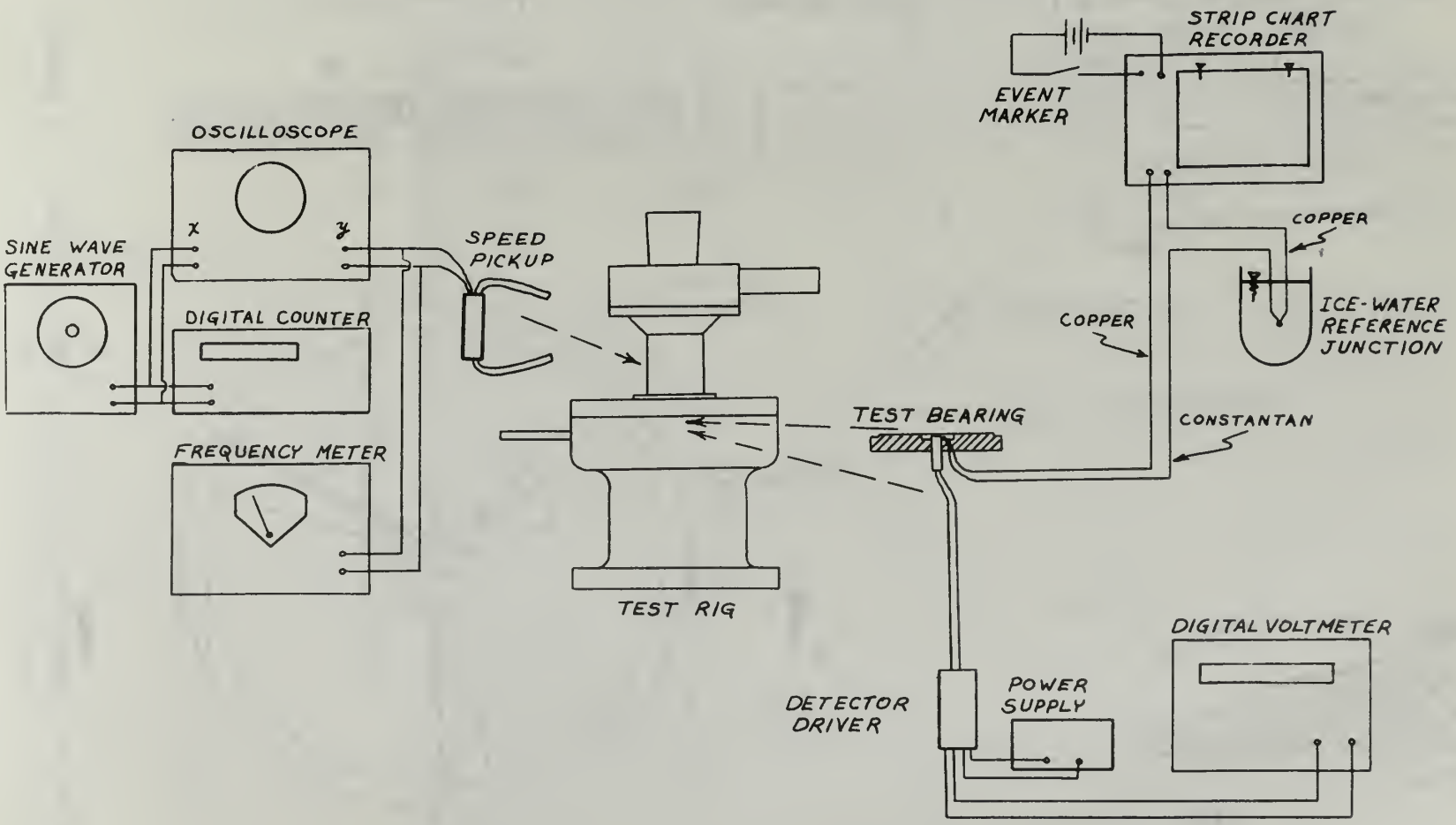

FIGURE 10. ELECTRONIC INSTRUMENTATION SCHEMATIC

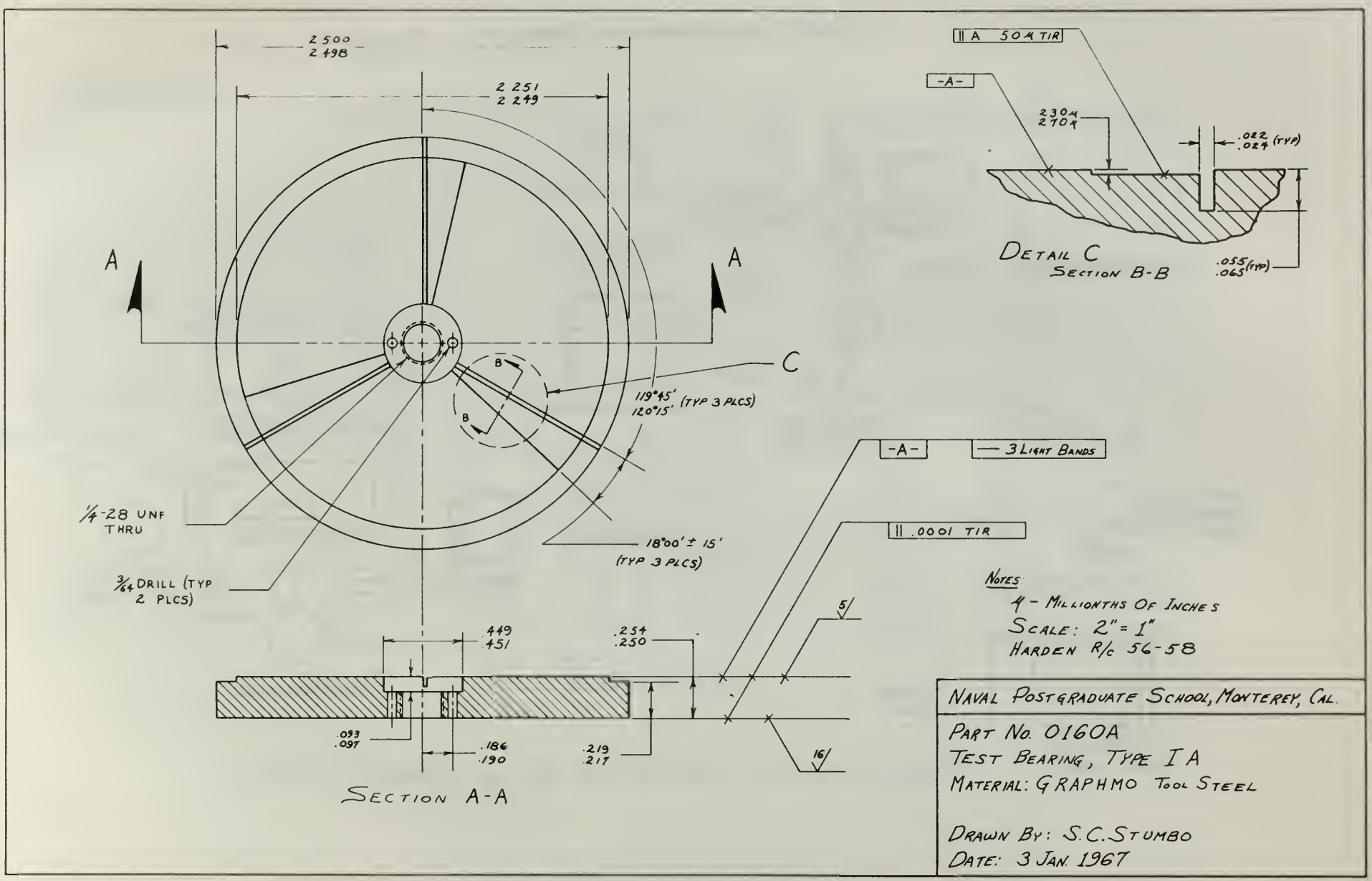

FIGURE II. TEST BEARING DESIGN

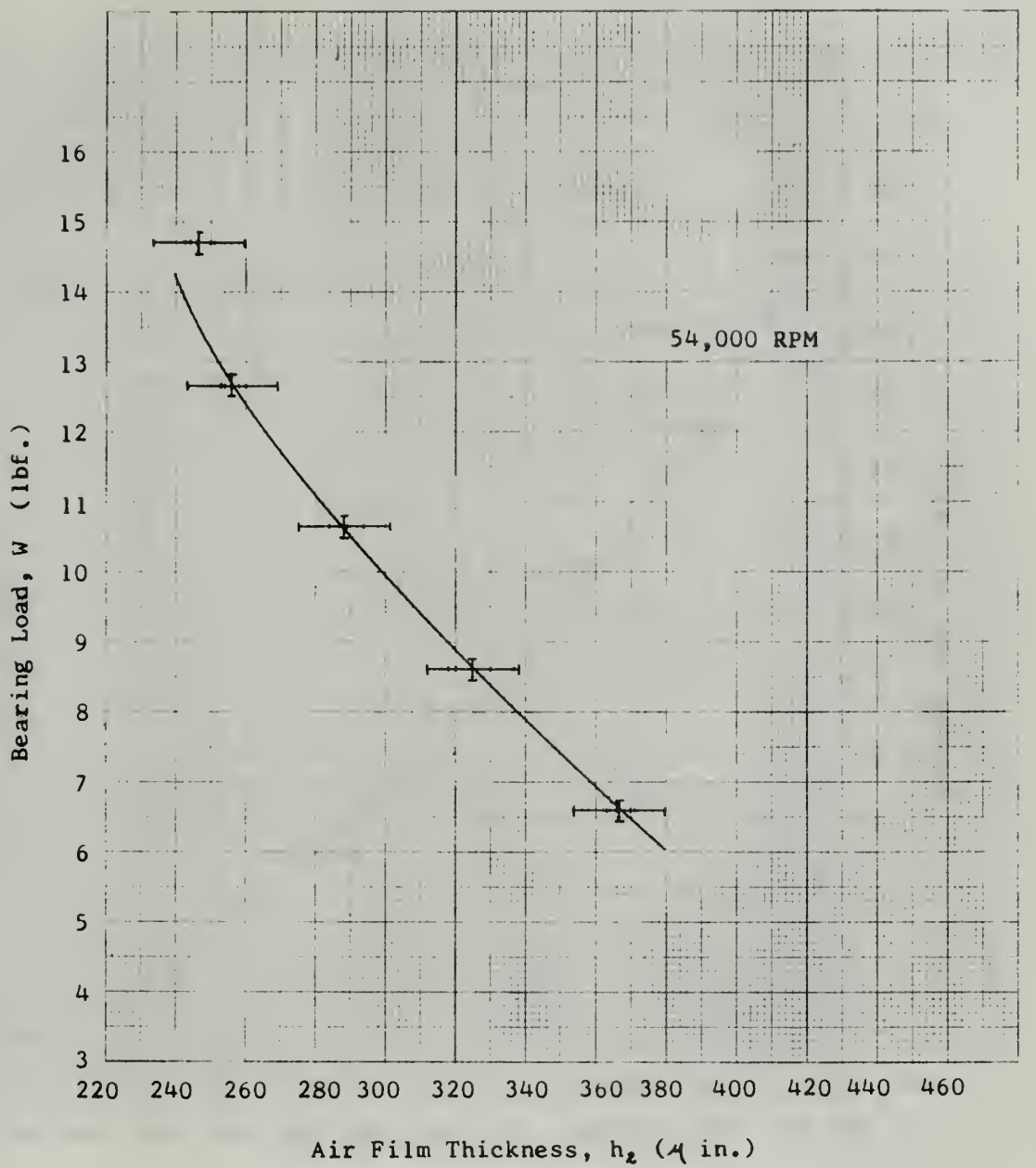

FIGURE 12. BEARING LOAD vs. AIR FILM THICKNESS - 54,000 RPM

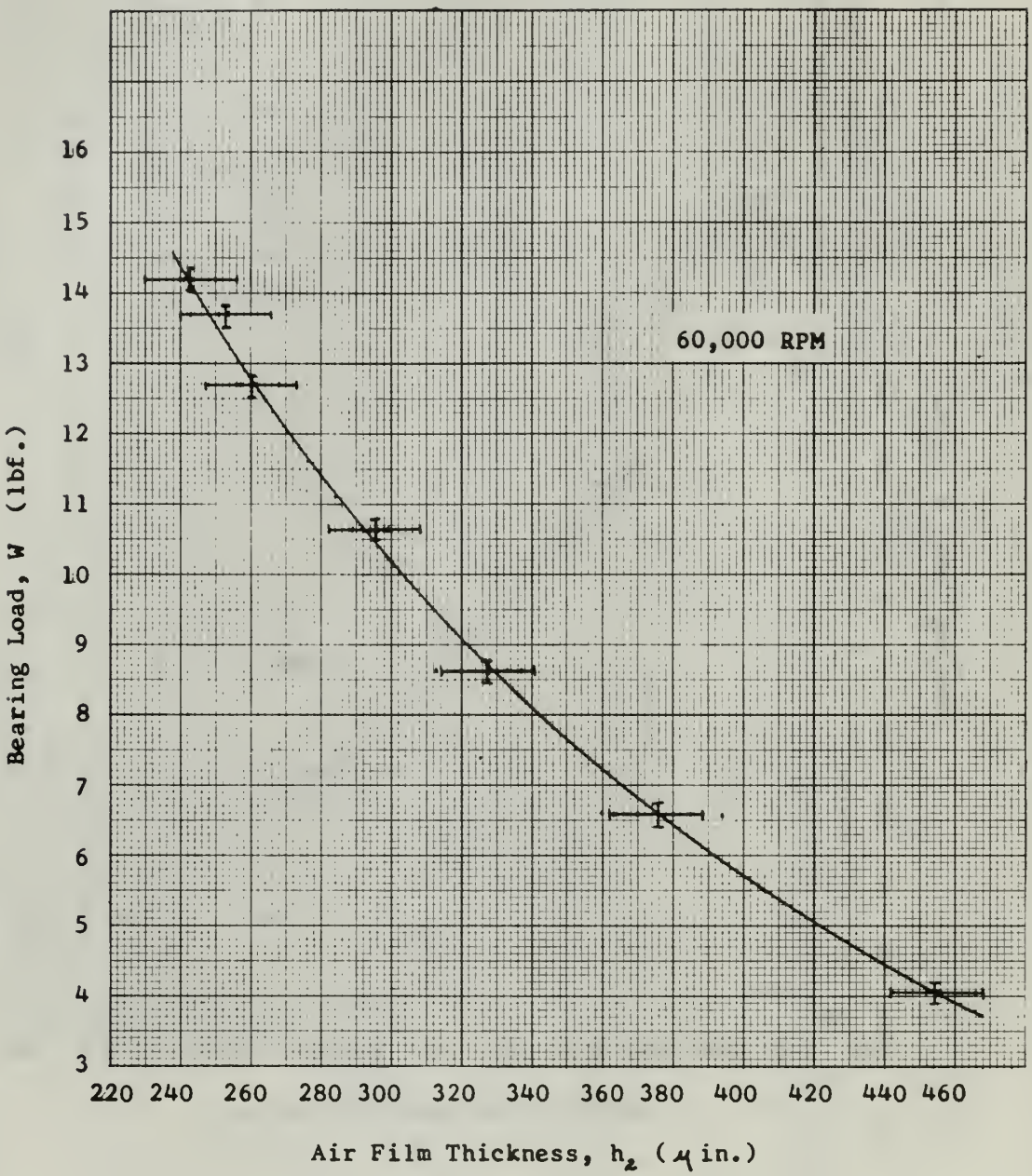

FIGURE 13. BEARING LOAD vs. AIR FILM THICKNESS - 60,000 RPM

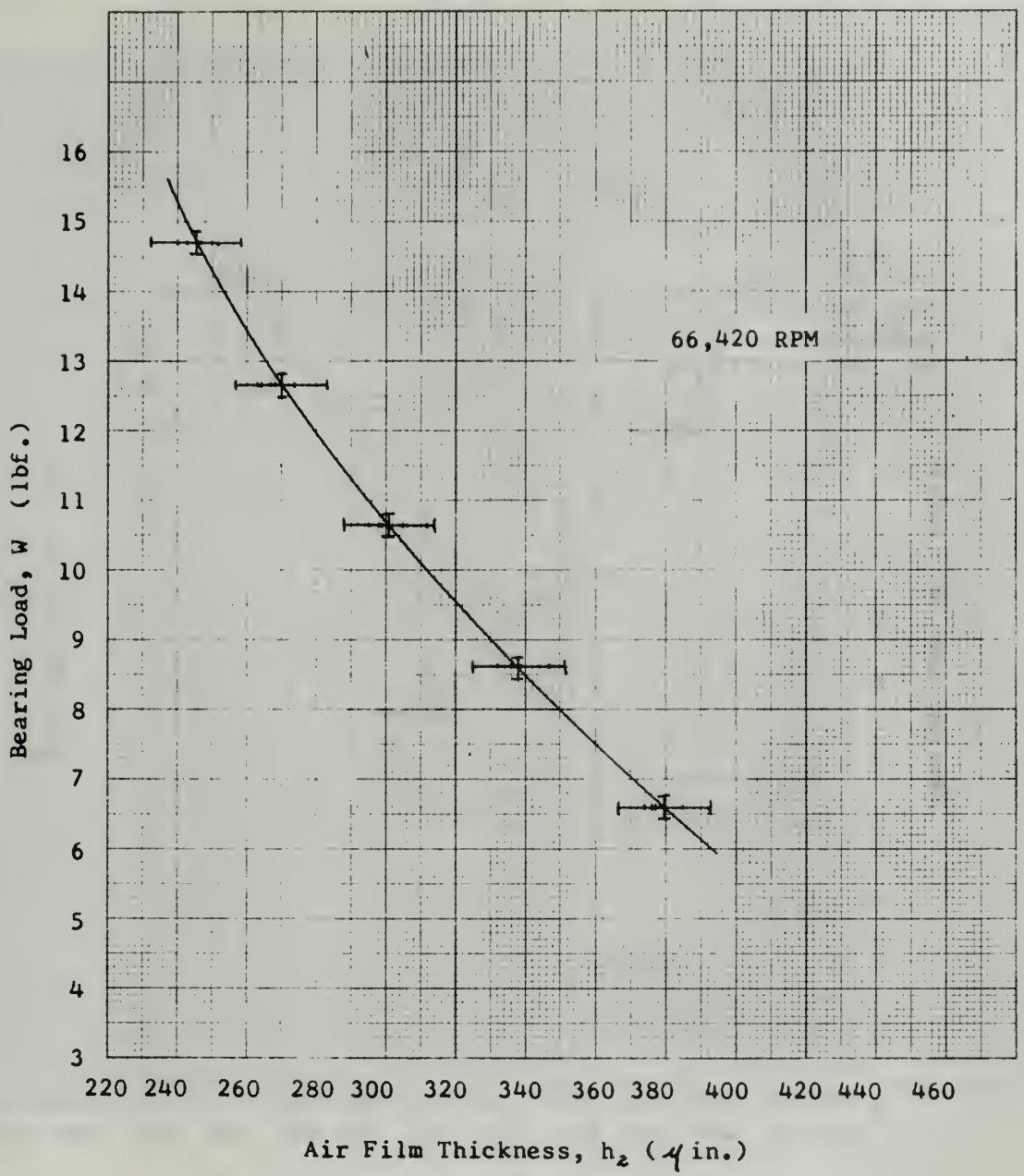

FIGURE 14. BEARING LOAD vs. AIR FILM THICKNESS - 66,420 RPM

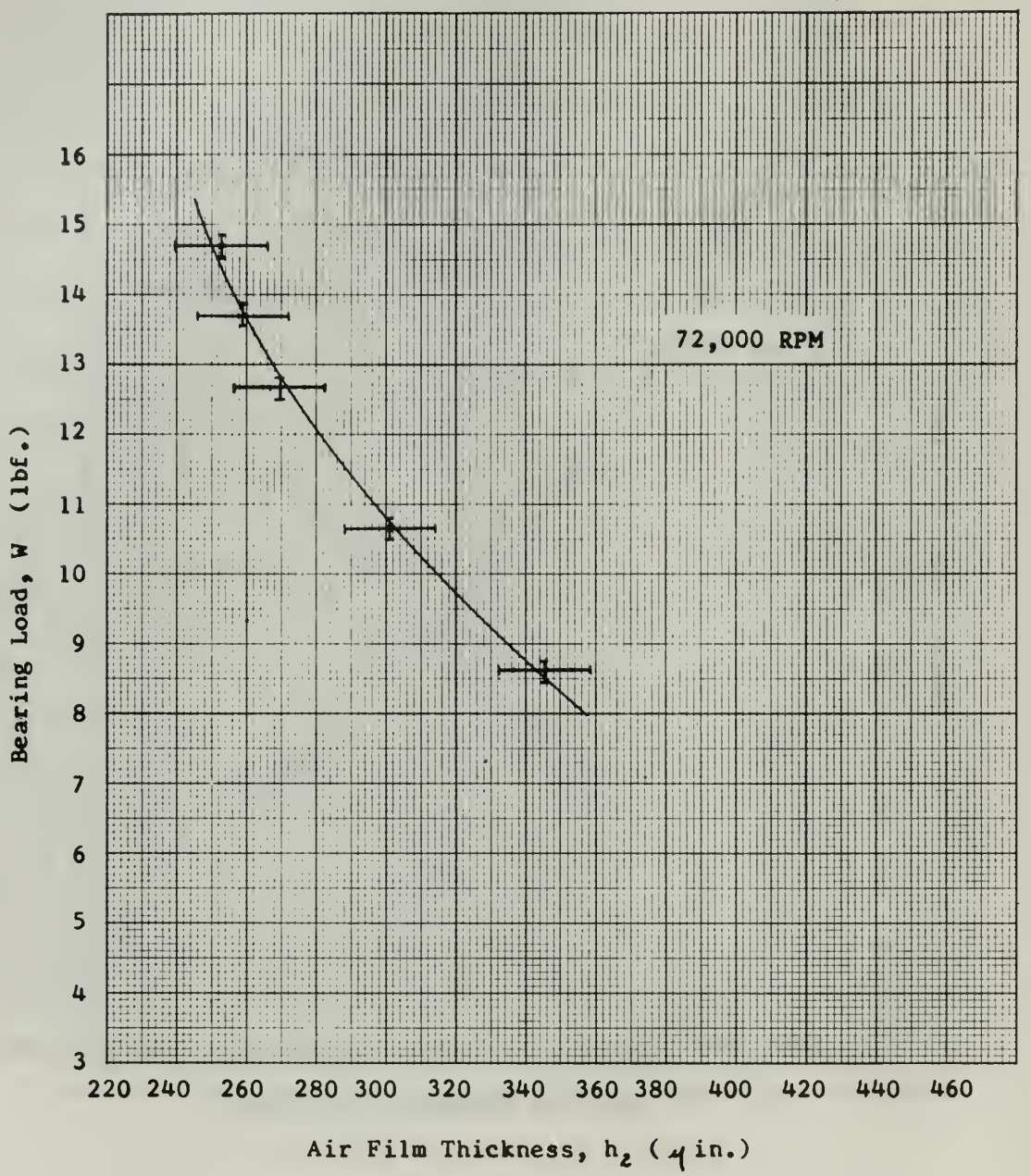

FIGURE 15. BEARING LOAD vs. AIR FILM THICKNESS - 72,000 RPM

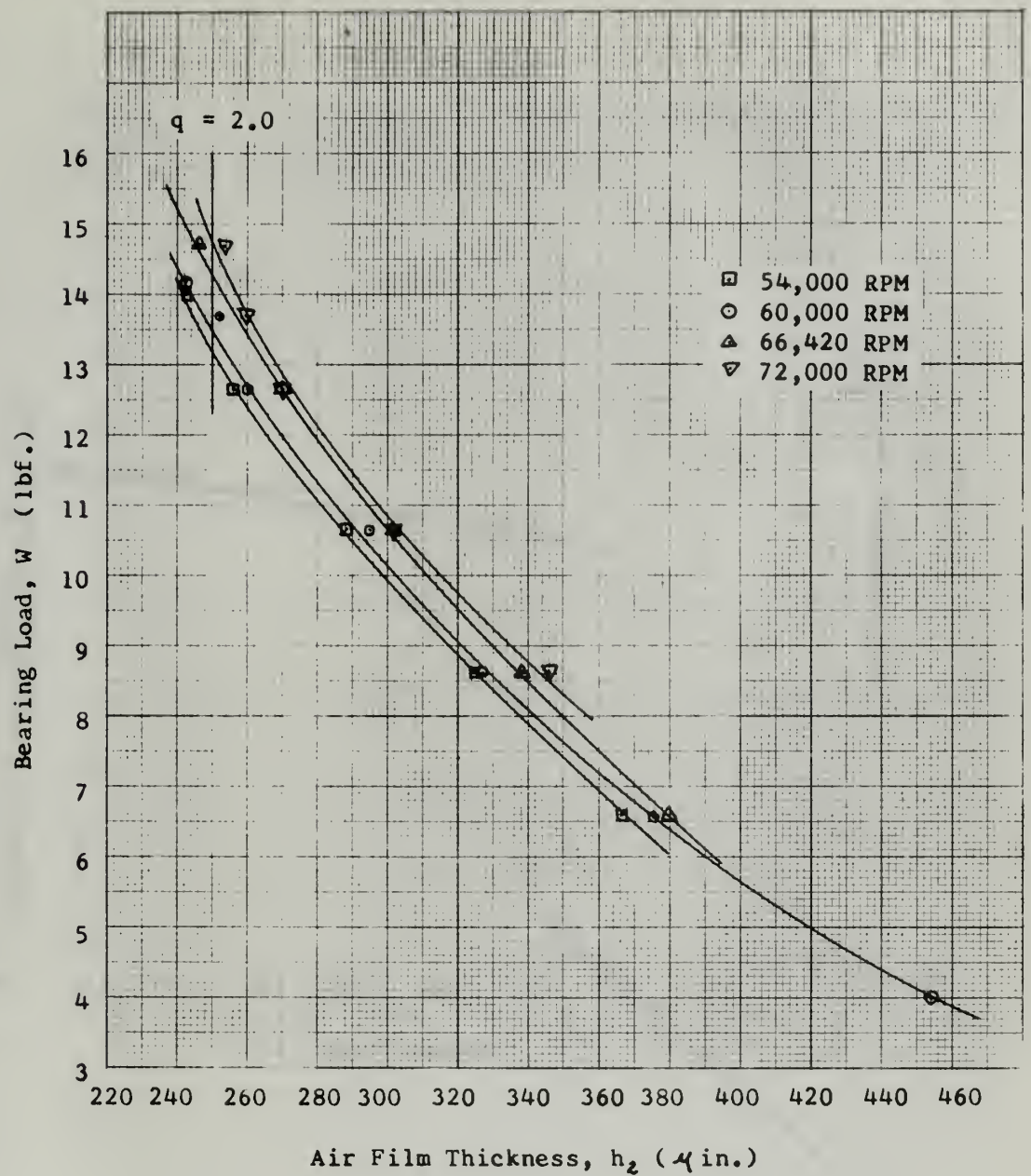

FIGURE 16. BEARING LOAD vs. AIR FILM THICKNESS AT VARIOUS SPEEDS

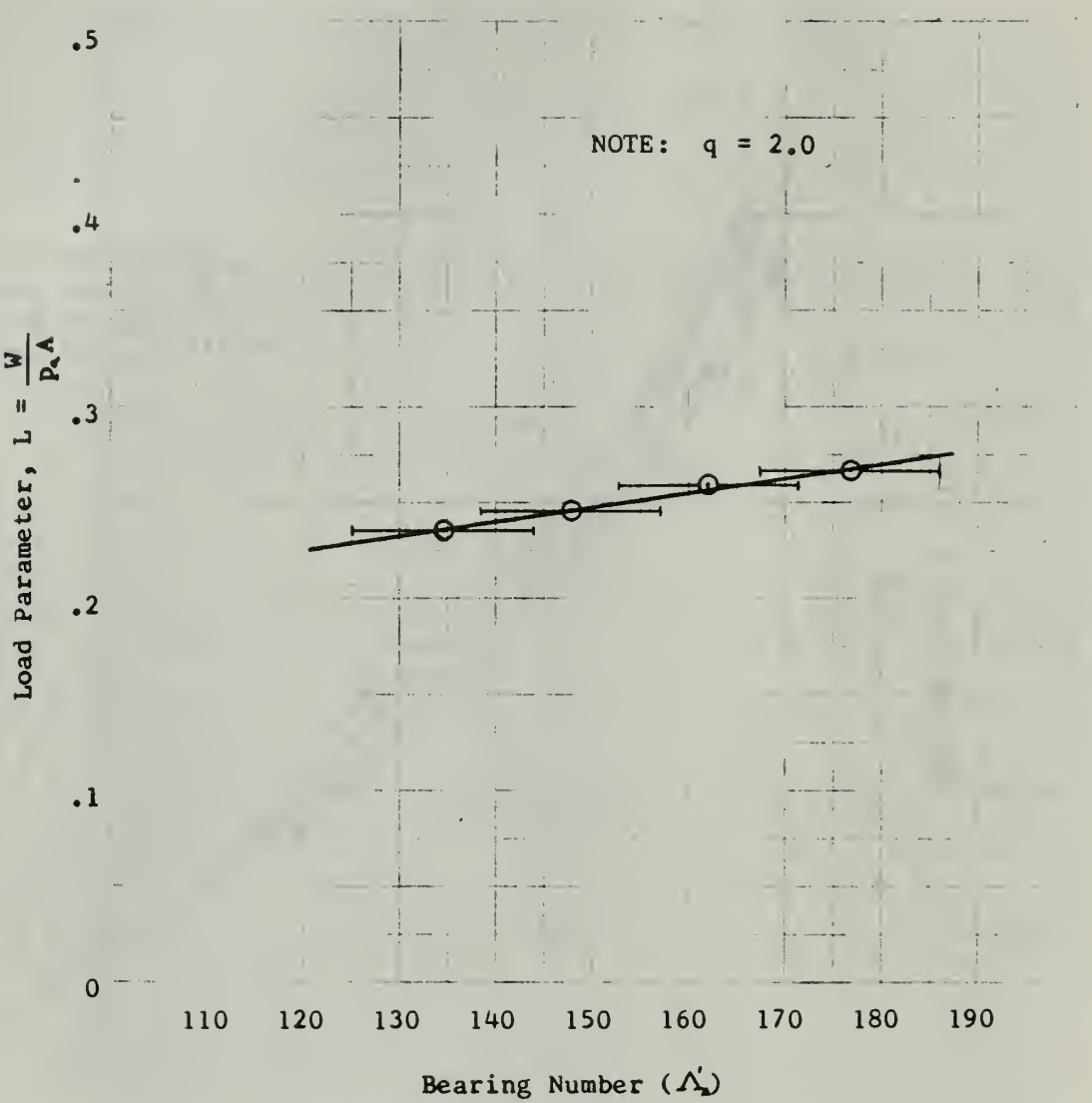

FIGURE 17. LOAD PARAMETER vs. MODIFIED BEARING NUMBER FOR q = 2 (TEST BEARING)

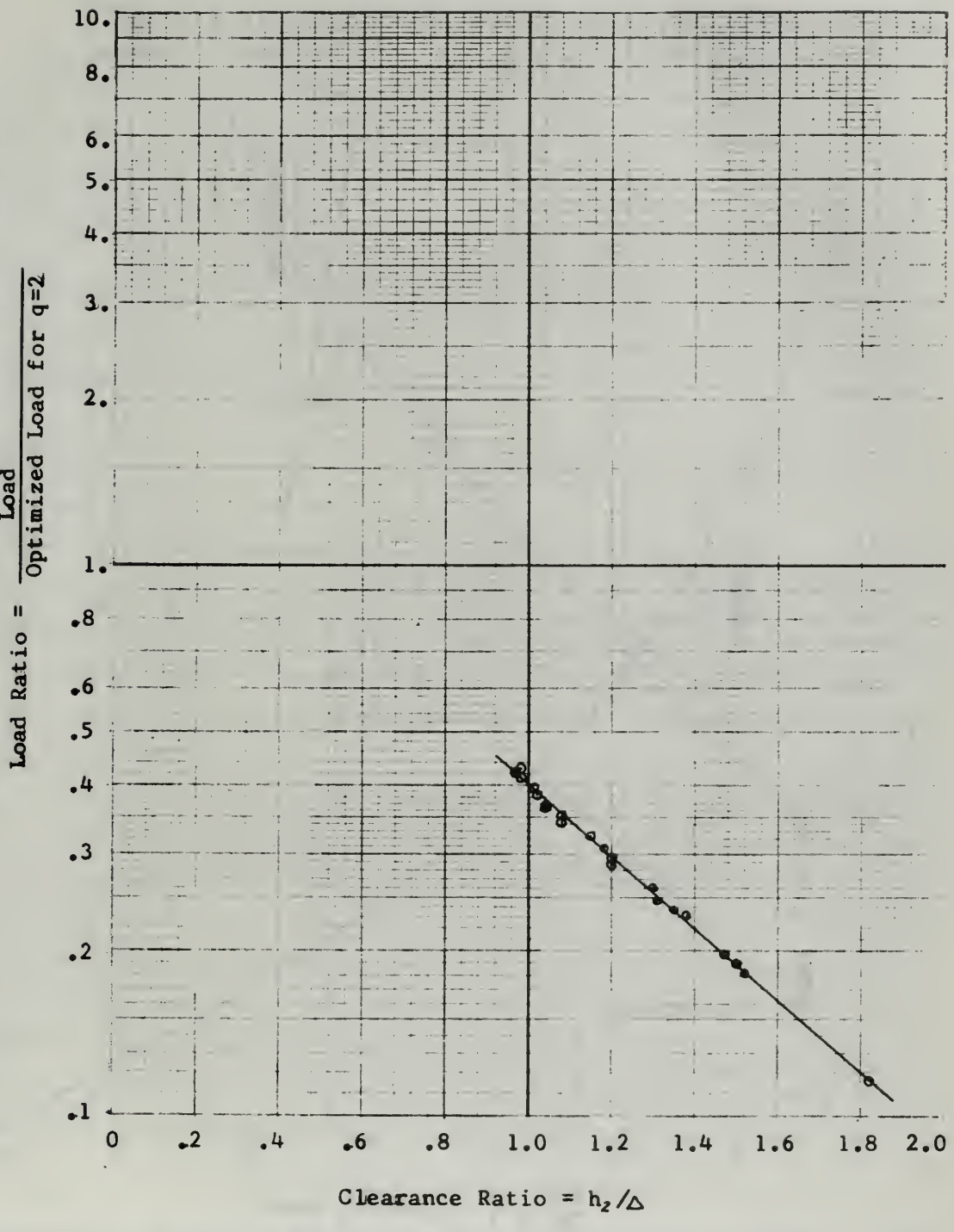

FIGURE 18. LOAD RATIO vs. CLEARANCE RATIO (TEST BEARING)

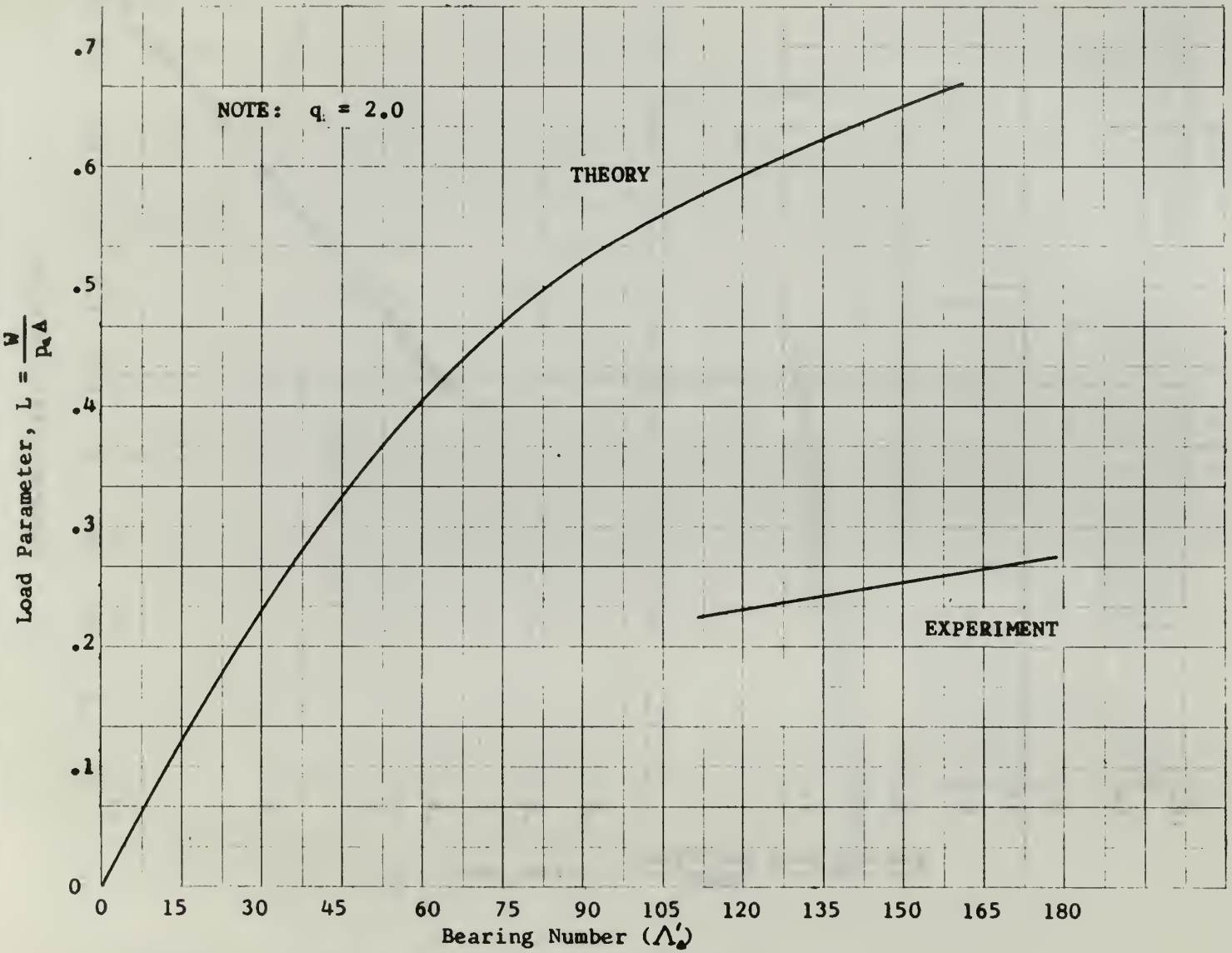

FIGURE 19. THEORETICAL AND EXPERIMENTAL LOAD CAPACITY

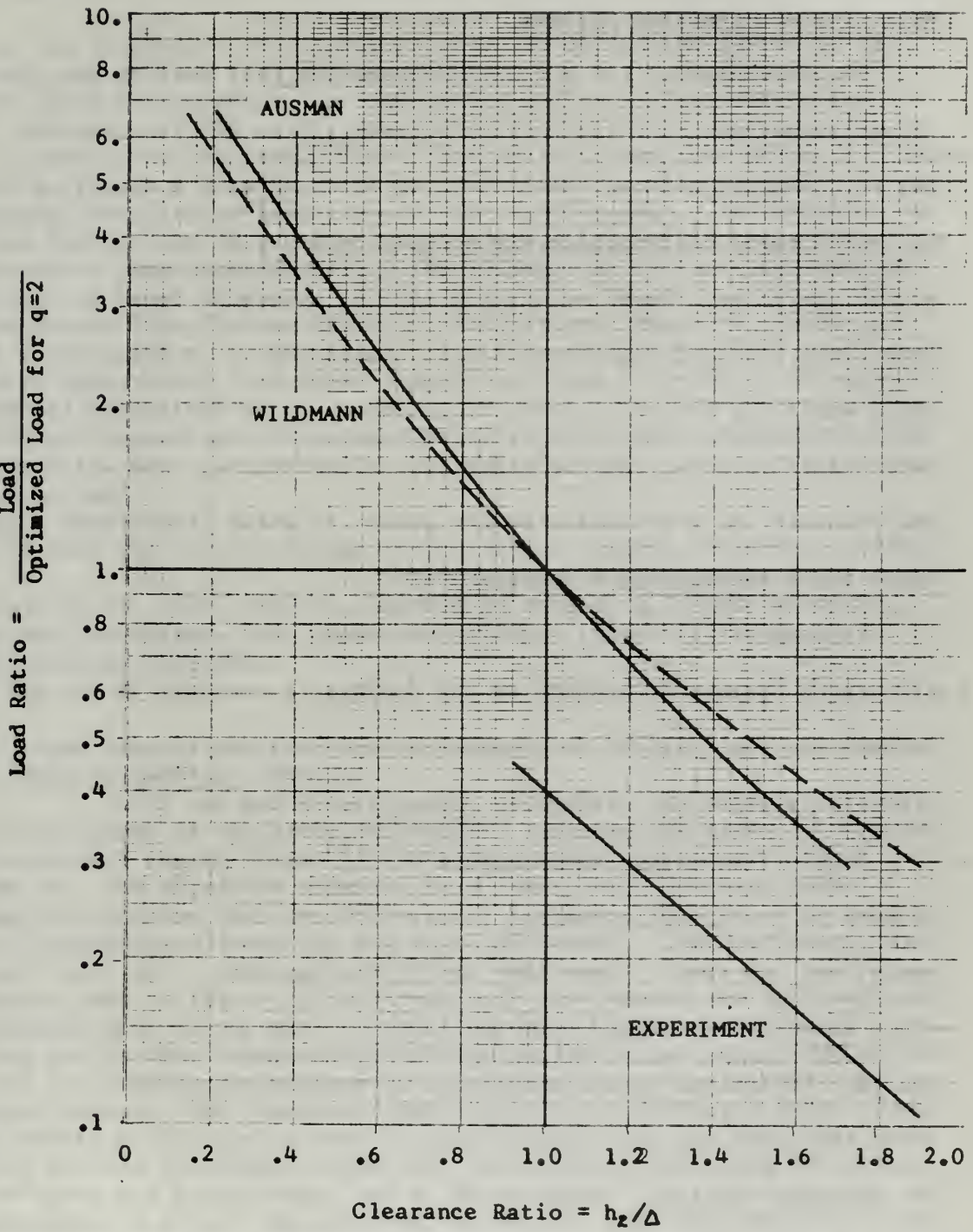

FIGURE 20. THEORETICAL AND EXPERIMENTAL LOAD RATIO vs. CLEARANCE RATIO

APPENDIX A

DISTANCE PROBE CALIBRATION

Selection of Measuring Systems

The thickness of the air film between the test bearing and its thrust runner was expected to vary between 150 to 400 microinches. It was felt that significant data could be obtained with a measuring technique which could discriminate within plus or minus 10 microinches during actual operation. Based on descriptions of apparatus found in the literature, two types of sensors should be considered --- a capacitance probe which would use the air film to be measured as the dielectric between two parallel plates, and the magnetic, or reluctance, type which senses the proximity of a conductor by the extent to which it disturbs a magnetic field surrounding a sensing coil.

Although it is capable of high accuracy, the capacitance type was eliminated because it depends on the dielectric constant of the air film. It was felt that changes in temperature and moisture content would unpredictably alter the dielectric properties of the air film.

Bently Proximitors manufactured by the Bently-Nevada Corp.were chosen because of their high potential accuracy, convenient mounting arrangements, and low cost. Since they are of the magnetic reluctance type, their measurements depend upon the nature of the conducting surface being sensed. Variations in the properties of nonconducting materials between the probe and the measured surface have no measurable effect on the accuracy obtained. Temperature of the probe itself was found to have an effect, however, even though silver-wound coils, advertised as the least temperature sensitive, were used.

Enhancement of Accuracy

The selected probes were intended to measure a range of 0 to .010 inches and to resolve to ± .0001 inches. To attain the necessary accuracy (± 10 microinches), the resolution had to be improved tenfold.

According to the manufacturer, the accuracy and resolution is directly proportional to the stability of the input voltage. Accordingly, an ultra-stable power supply meeting the voltage and current requirements was purchased from Systems Research Corporation. Measured ripple and noise of their Model 3566 Power Supply was found to be 50 to 80 microvolts peak to peak and the output varied no more than 1.0 millivolts in a 24 hour test.

To read the output voltage accurately, a digital voltmeter, Electro Instruments Co. Model DVX-500, capable of measuring to the nearest 0.1 millivolts was obtained.

Probe Calibration Methods

Photographs of the probe calibration rig used are shown in Figures A1 and A2. The apparatus consists of a Johannson Mikrokator Model S 510E-7 Comparator altered for use as a calibrator. The Mikrokator dial indicator seen in Figure A2 is accurate to the nearest one millionth of an inch and is thus capable of establishing the actual resolution of the distance probes. The comparator was altered by providing a rigid clamp fixture to hold a distance probe over the movable table, and by making arrangements to adjust the position of the dial indicator head by means of a fine adjustment mechanism salvaged from a microscope.

The surface to which the probes were calibrated was the surface of a disc made indentical to the thrust runner actually used in the thrust bearing test rig. This was done by cutting the disc from the same billet

of steel and having it follow the shaft with thrust runner through the same machining, heat treating, grinding and lapping processes.

Provisions were made for checking the effects of temperature on the distance measurements. The ambient temperature was accurately recorded before, during, and after each calibration. The calibration rig was allowed to "soak" for at least three hours at any given temperature to eliminate any transient expansion or contraction.

A temperature sensitivity test was performed to insure that temperature changes in readout were not due to mere distance changes as a result of expansion or contraction of clamping fixtures of the calibration rig itself. A probe was clamped in a vertical position with its sensing surface up. The test surface disc was allowed to rest above the probe face with a separation of .015 inches maintained by a thin sheet of Pyrex glass. The coefficient of thermal expansion, α , of Pyrex glass is $2.0 \times 10^{-6} \frac{\text{in.}}{\text{in.}^\circ\text{F.}}$ So for a temperature change of 100F, for instance, the glass thickness ,a , will change by

$$\Delta a = \alpha a (\Delta t)$$

$$= (2.0 \times 10^{-6})(.015)(100)$$

$$= 3.0 \text{ microinches}$$

This arrangement was then subjected to heated air blown from a portable heat gun while the output reading was watched for deviation.

Results

In the temperature sensitivity test, raising the temperature approximately 50F caused a change in reading of about 100 millivolts. This represents a relative distance change of about 140 microinches and conclusively confirmed suspicions that the probes themselves are affected by

temperature.

Calibration curve data are presented in Tables A1-A3. The resulting calibration curves are presented in Figure A3. Note that data was taken only in a small linear region of the probe's effective range since larger displacement measurements were not anticipated. The slope of the curves was the same in every case:

$$\text{Slope} = 1.4118 \frac{\text{microinches}}{\text{millivolt}}$$

Discussion

From Figure A3 it is immediately apparent that although temperature changes affect the position of the curve, only the zero, or reference, point is affected. The slope of the curve remains constant over the expected range of measurements. Accordingly, the experimental procedure during actual runs included the determination of a zero point (bearing and thrust runner in contact) immediately after each run while the rig and probe were still at operating temperature. Measurements were then taken from this zero point using the constant slope of the calibration curves.

To determine data scatter and accuracy, the data was originally plotted on 20x24 inch graph paper with 10x10 squares to the half-inch. The mean deviation from the straight line plots was 0.96 microinches. Thus by accuracy and stability enhancements, together with careful calibration, the resulting data may be considered reliable within $\pm$ 1.92 microinches, or twice the mean deviation. This is better than five times the necessary accuracy and fifty times better than the manufacturer's intended accuracy.

TABLE A1

DISTANCE PROBE CALIBRATION DATA

68.6°F

Run No.	Relative Distance (in.)	Probe Output (mv)
1	400	6069
	379	6035
	337	6000
	296	5968
	268	5945
	204	5900
	170	5875
	121	5838
	66	5800
	3	5756
2	392	6056
	359	6031
	320	6005
	271	5968
	216	5933
	168	5896
	111	5857
	63	5820
	9	5777

TABLE A2

DISTANCE PROBE CALIBRATION DATA

75.4°F

Run No.	Relative Distance (in.)	Probe Output (mv)
3	398	5943
	350	5907
	302	5874
	251	5836
	193	5795
	139	5759
	95	5724
	52	5695
4	398	5941
	344	5898
	310	5872
	229	5815
	176	5777
	114	5731
	62	5689
	0	5648

TABLE A3

DISTANCE PROBE CALIBRATION DATA

49.4°F

Run No.	Relative Distance (in.)	Probe Output (mv)
5	396	6242
	366	6219
	307	6175
	254	6134
	234	6123
	177	6082
	217	6037
	68	6005
	0	5956
6	395	6207
	360	6186
	310	6154
	251	6117
	207	6088
	158	6054
	123	6028
	87	6004
	51	5981
	18	5956
	0	5942

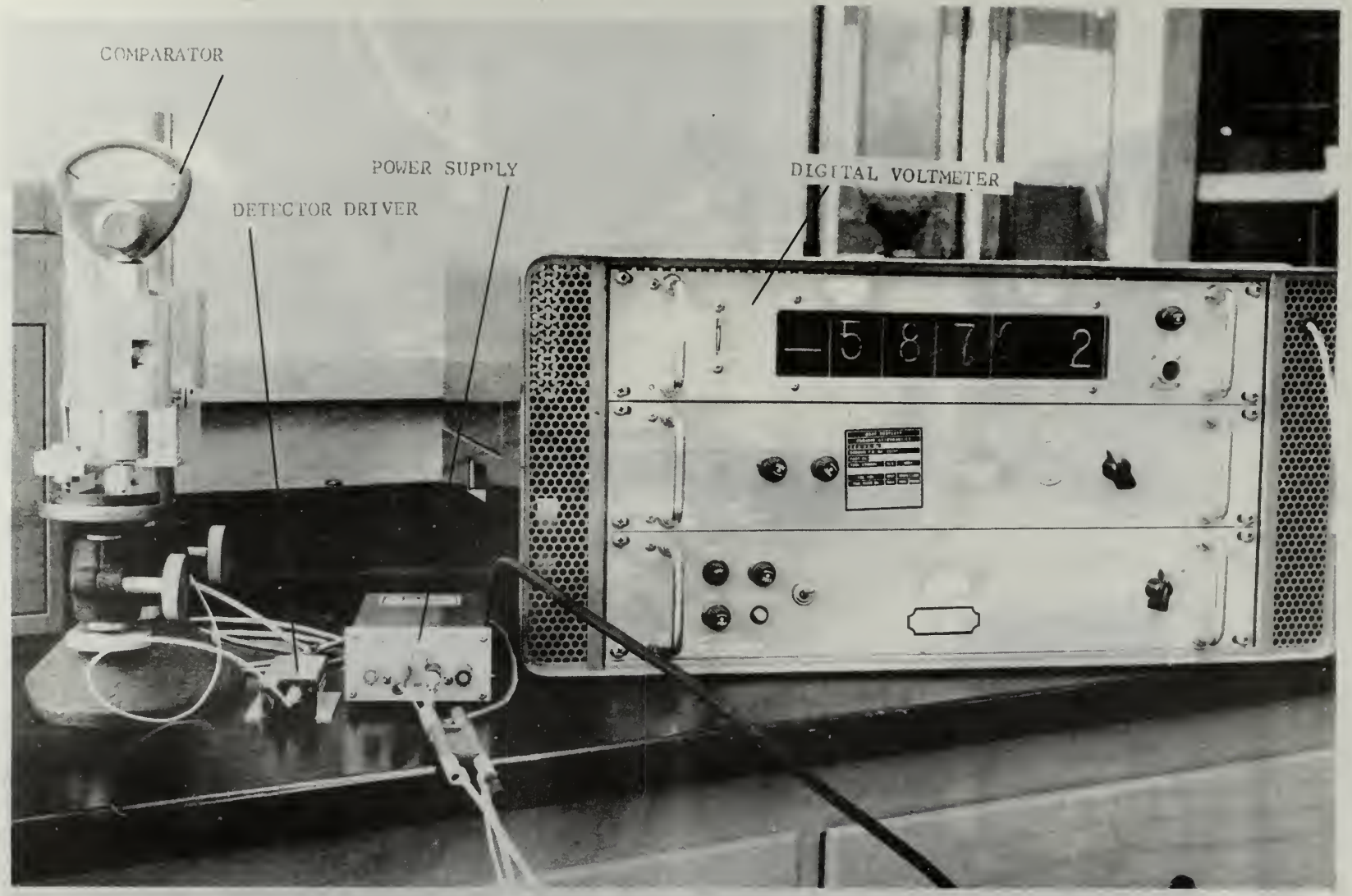

FIGURE A1. DISTANCE PROBE CALIBRATION APPARATUS

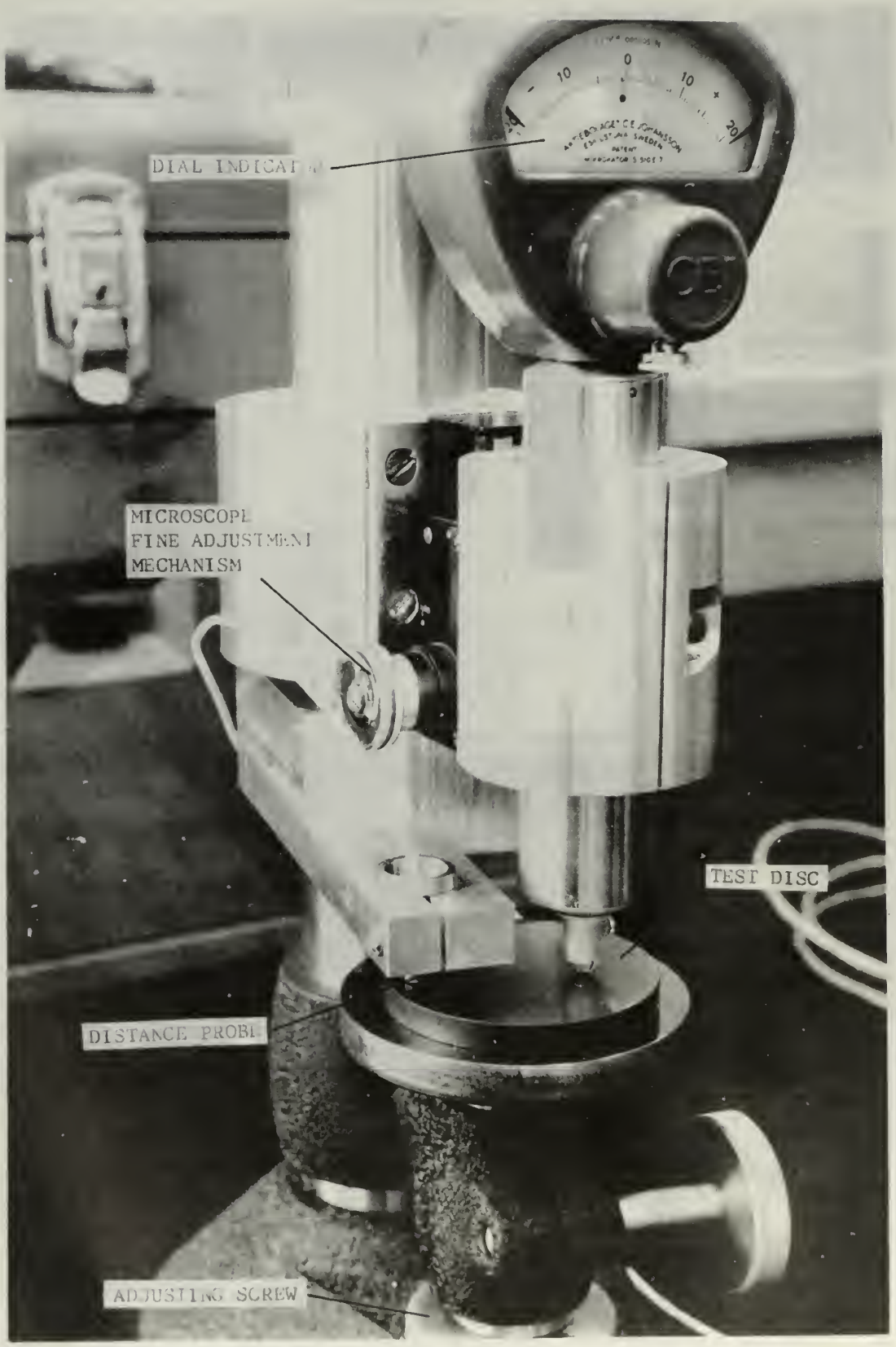

FIGURE A2.1 CALIBRATION DISC AND PROBE IN PLACE ON COMPARATOR

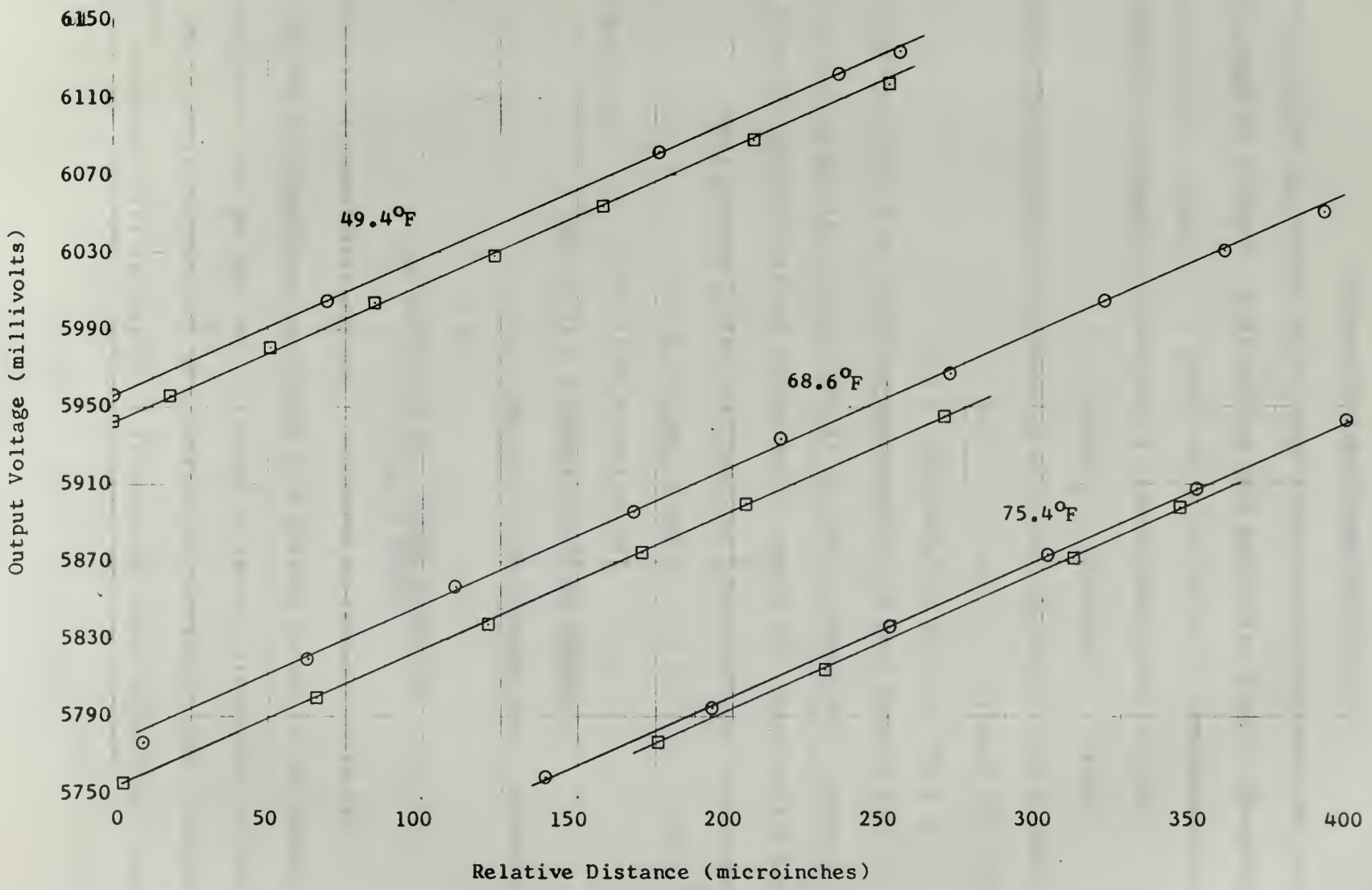

FIGURE A3. DISTANCE PROBE CALIBRATION CURVES

APPENDIX B

DATA REDUCTION CALCULATIONS

The results of measurements shown in the Summary of Data (Tables 1 through 4) were calculated from the raw data. Examples of these calculations follow.

Since the speed measurement is indicated by a frequency (hertz) and

1 hertz = 1 revolution per second

speed in revolutions per minute is computed by multiplying this value by 60. For example:

N = 900 hz. x 60 = 54,000 rpm

The bearing load is indicated by the height of a column of mercury in inches. The manometer reading is converted to psi and multiplied by the piston area. The weight of the piston and test bearing assembly is subtracted from the result to obtain the actual bearing load:

2.036 in. Hg = 1.0 psi

Piston Area = 10.317 in.

Weight of Piston Assembly = 11.65 lbs.

Therefore, for a reading of 4.0 in. Hg,

$$W = \frac{4.0 \times 10.317}{2.036} - 11.65 = 8.62 \text{ lbs.}$$

Air film thickness is determined from the difference (in millivolts) between the voltmeter reading at a particular speed and load and the reading immediately thereafter taken with the bearing and thrust disc in contact. This difference is multiplied by the constant slope of the probe calibration curve (Appendix A) to obtain air film thickness. From Run No. 14-1,

$$h_{\ell} = (5864 - 5607)(1.4118)$$

$$= 257 \times 1.4118 = 363 \text{ microinches}$$

Subsequent analysis of the results is performed using the dimensionless parameters, Λ_{ℓ}, L, ω, and Load Ratio (L/L_{ℓ}). The calculation of these parameters is described in the following paragraphs.

The bearing number, Λ'_{ℓ}, is

$$\Lambda'_{\ell} = \frac{\mu \omega R^2}{p_a \Delta^2}(1-b^2)$$

where constant values are

$\mu = 28 \times 10^{-10}$ reyns

R = 1.125 in.

$\Delta = 25.0 \times 10^{-5}$ in.

b = 0.2

and

$\omega = \left(\frac{N}{60}\right) 2\pi$ rad/sec

p = barometric pressure (in. Hg) x .4912 $\frac{\text{psi}}{\text{in. Hg.}}$

For Run No. 6,

$\omega = 1000\ (2\pi) = 6283$ rad./sec.

p = 30.31 x .4912 = 14.89 psia

and

$$\Lambda'_{\ell} = \frac{(6)(28 \times 10^{-10})(6283)(1.125^2)}{(14.89)(25 \times 10^{-5})^2}\ (1 - .2^2)$$

$$= 137.8$$

The load parameter, L, is given by

$$L = \frac{W}{p_a A}$$

where

$$A = (R^2 - r_i^2)\pi \times (354/360)$$

$$= (1.125^2 - .225^2)\ \pi\ (354/360)$$

$$= 3.755 \text{ in.}$$

The fraction 354/360 accounts for the fact that the air inlet grooves are not part of the load carrying area. Again for Run No. 6,

$$L = \frac{12.67}{(14.89)(3.755)}$$

$$= 0.227$$

The clearance ratio, $\alpha = h_2/\Delta$, is computed from the average film thickness for a given run. Using Run No. 6,

$$h_2(\text{avg}) = 259.7 \text{ microinches}$$

and

$$\alpha = \frac{259.7}{250} = 1.04$$

The optimized load for q = 2 is found by consulting Figure 3 for the particular bearing number, Λ'_Δ . For example if

$$\Lambda'_\Delta = 137.8$$

$$L = .628$$

and

$$\text{Load Ratio} = \frac{.227}{.628} = .361$$

APPENDIX C

EXPERIMENTAL UNCERTAINTY INTERVALS

Reference [9] gives the uncertainty interval for a result as

$$w_R = \left[\left(\frac{\partial R}{\partial v_1} w_1\right)^2 + \left(\frac{\partial R}{\partial v_2} w_2\right)^2 + \cdots + \left(\frac{\partial R}{\partial v_n} w_n\right)^2\right]^{1/2}$$

where w_1, w_2, ..., w_n are the uncertainty intervals of the variables making up the result, R is the expression for the result, and v_1, v_2, ..., v_n are the variables making up the result.

The expression for bearing load is

$$W = p A_p - W_p$$

where

p = load pressure (in. Hg)

A_p = piston area (in.)

W_p = weight of piston & test bearing assembly (lbm.)

The uncertainty interval for bearing load is

$$w_W = \left[\left(\frac{\partial W}{\partial p} w_p\right)^2 + \left(\frac{\partial W}{\partial A_p} w_{A_p}\right)^2 + \left(\frac{\partial W}{\partial W_p} w_{W_p}\right)^2\right]^{1/2}$$

Dividing through by W to nondimensionalize the equation results in

$$\frac{w_W}{W} = \left[\left(\frac{w_p}{p}\right)^2 + \left(\frac{w_{A_p}}{A_p}\right)^2 + \left(\frac{w_{W_p}}{W_p}\right)^2\right]^{1/2}$$

For

p_L = 4.4 $\pm$ .05 in. Hg (20 to 1)

A_p = 10.317 $\pm$ .001 in. (20 to 1)

W_p = 11.65 $\pm$ .02 lbm (20 to 1)

$$\frac{w_W}{10.65} = \left[\left(\frac{.05}{4.4}\right)^2 + \left(\frac{.001}{10.317}\right)^2 + \left(\frac{.02}{11.65}\right)^2\right]^{1/2}$$

$$= .01544$$

and

$$w_{w7} = (10.65)(.01544) = \pm 0.164 \text{ lbf.}$$

Air film thickness is computed in the following way:

$$h_2 = (V_1 - V_2)S$$

where

V_1 = probe output voltage at speed and load (mv)

V_2 = probe output voltage at zero point (mv)

S = slope of probe calibration curve (μ in./mv)

One additional factor must be taken into account. Inspection of the probe calibration curves shows an average temperature sensitivity of 14 mv/°F at a constant distance between probe and measured surface. Examination of all temperature data taken shows that in only one out of ten readings did the probe temperature differ at speed and load from the zero point by more than 1.25 °F. An actual temperature trace from the strip chart recorder is shown as Figure C-1. Defining an additional error,

w_{vT} = uncertainty interval due to a difference in probe temperatures

$= (14.0)(1.25)$

$= \pm 17.5$ mv

It is felt by the writer that repetition of each data point an average of six times halved this uncertainty interval at the very least. The interval used is

$$w_{vT} = \pm 8.75 \text{ mv} \qquad (10 \text{ to } 1)$$

Therefore for Run No. 5-2 using the previous method,

$$\frac{w_{h_2}}{h_2} = \left[\left(\frac{w_{V_1}}{V_1}\right)^2 + \left(\frac{w_{V_2}}{V_2}\right)^2 + \left(\frac{w_{vT}}{V_1 - V_2}\right)^2 + \left(\frac{w_s}{S}\right)^2\right]^{1/2}$$

where

V_1 = 5788 ± 2 mv (20 to 1)

V_2 = 5580 ± 2 mv (20 to 1)

S = 1.4118 ± .0054 in./mv (20 to 1)

and

$$\frac{w_{h_2}}{.294} = \left[\left(\frac{2}{5788}\right)^2 + \left(\frac{2}{5580}\right)^2 + \left(\frac{.675}{208}\right)^2 + \left(\frac{.0054}{1.4118}\right)^2\right]^{1/2}$$

w_{h_2} = 294(.0422)

= 12.41 microinches

The expression for bearing number is

$$\Lambda_2 = \frac{6\mu\omega R^2}{p_a \Delta^2}\left(1 - b^2\right)$$

and by similar means

$$\frac{w_{\Lambda_2}}{\Lambda_2} = \left[\left(\frac{w_\mu}{\mu}\right)^2 + \left(\frac{w_\omega}{\omega}\right)^2 + \left(\frac{w_{p_a}}{p_a}\right)^2 + 2\left(\frac{w_\Delta}{\Delta}\right)^2\right]^{1/2}$$

where for Run No. 5-2,

μ = 28×10^{-10} ± 1×10^{-10} reyns (20 to 1)

ω = 6283 ± 6.283 rad./sec. (20 to 1)

p_a = 30.31 ± .01 in. Hg (20 to 1)

Δ = 250 ± 10 microinches (20 to 1)

and

$$\frac{w_{\Lambda_2}}{137.8} = \left[\left(\frac{1}{28}\right)^2 + \left(\frac{6.283}{6283}\right)^2 + \left(\frac{.01}{30.31}\right)^2 + 2\left(\frac{10}{250}\right)^2\right]^{1/2}$$

w_{Λ_2} = 137.8(.0669)

= ± 9.22

Similarly for Run No. 5 (averaged points),

Λ = h_2/Δ

$$\frac{w_\alpha}{\alpha} = \left[\left(\frac{w_{h_2}}{h_2}\right)^2 + \left(\frac{w_\Delta}{\Delta}\right)^2\right]^{1/2}$$

$$\frac{w_\alpha}{1.18} = \left[\left(\frac{12.41}{294}\right)^2 + \left(\frac{10}{250}\right)^2\right]^{1/2}$$

$$w_\alpha = 1.18\ (.0581)$$

$$= \pm .069$$

The foregoing are examples of the determination of uncertainty intervals for each data point. These intervals are represented on all graphical presentations of data as short lines through the data points in the following manner:

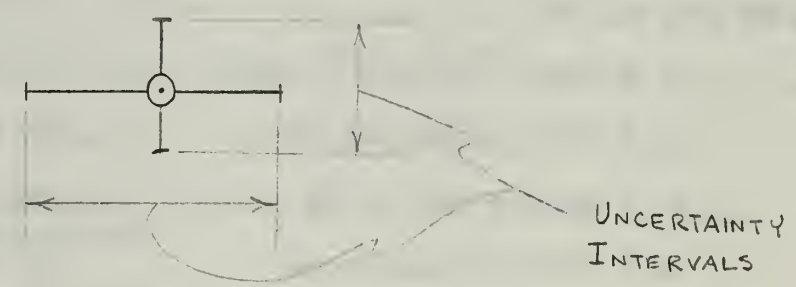

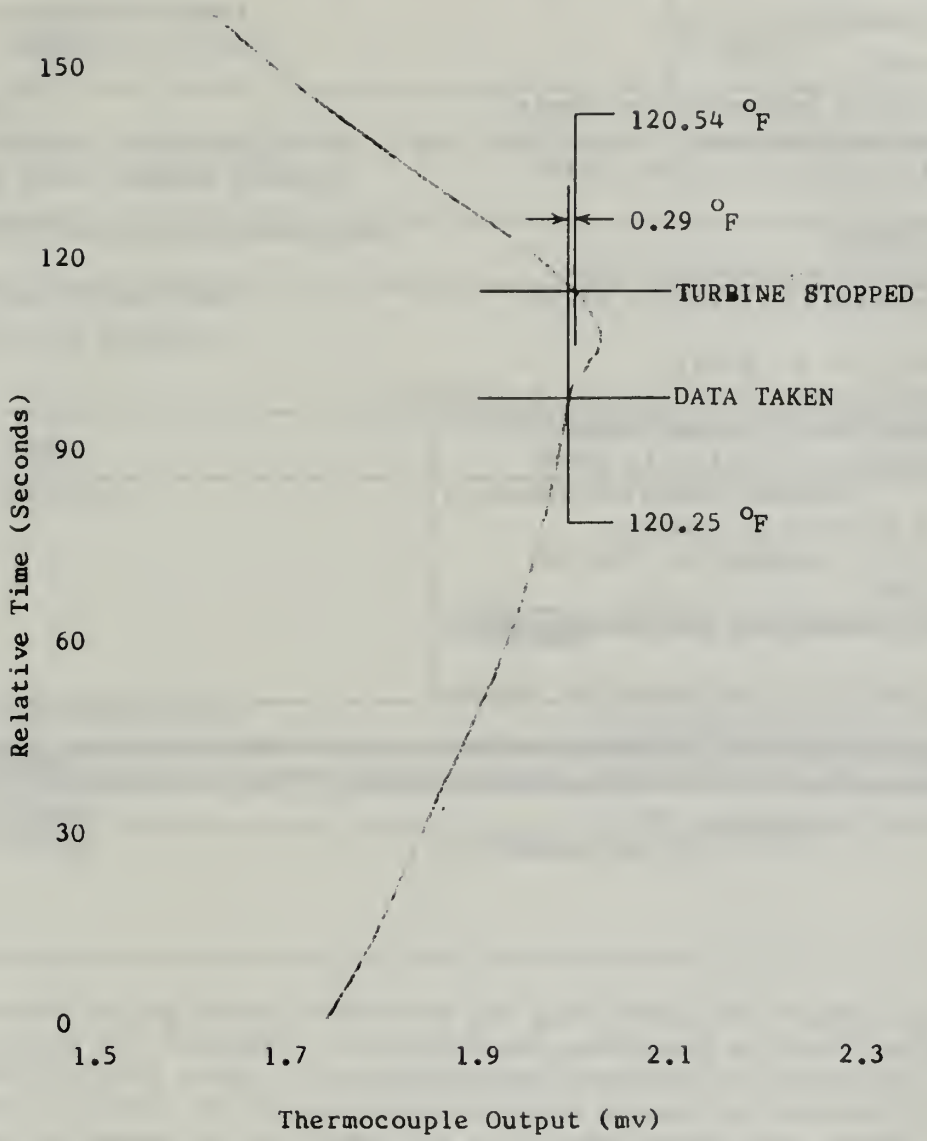

FIGURE C1. PROBE TEMPERATURE AS A FUNCTION OF TIME FOR RUN NO. 17-4

INITIAL DISTRIBUTION LIST

		No. Copies
1.	Defense Documentation Center Cameron Station Alexandria, Virginia 22314	20
2.	Library Naval Postgraduate School Monterey, California 93940	2
3.	Prof. P. F. Pucci Department of Mechanical Engineering Naval Postgraduate School Monterey, California 93940	5
4.	LT Stanley C. Stumbo U.S.S. BENNINGTON (CVS-20) % FPO San Francisco, California 96601	1
5.	AiResearch Manufacturing Company 9851-9951 Sepulveda Blvd. Los Angeles, California 90009 Attn: Department 93-17	1

DOCUMENT CONTROL DATA - R&D

(Security classification of title, body of abstract and indexing annotation must be entered when the overall report is classified)

1. ORIGINATING ACTIVITY (Corporate author)
Naval Postgraduate School
Monterey, California 93940

2a. REPORT SECURITY CLASSIFICATION
Unclassified

2b. GROUP
N/A

3. REPORT TITLE
AN EXPERIMENTAL INVESTIGATION OF A GAS LUBRICATED STEPPED SECTOR THRUST BEARING AT HIGH BEARING NUMBERS

4. DESCRIPTIVE NOTES (Type of report and inclusive dates)

5. AUTHOR(S) (Last name, first name, initial)
STUMBO, Stanley Charles

6. REPORT DATE
June 1967

7a. TOTAL NO. OF PAGES
80

7b. NO. OF REFS
9

8a. CONTRACT OR GRANT NO.

b. PROJECT NO.

c.

d.

9a. ORIGINATOR'S REPORT NUMBER(S)

9b. OTHER REPORT NO(S) (Any other numbers that may be assigned this report)

10. AVAILABILITY/LIMITATION NOTICES
This document is subject to special export controls and each transmittal to foreign nationals may be made only with prior approval of the Naval Postgraduate School.

11. SUPPLEMENTARY NOTES

12. SPONSORING MILITARY ACTIVITY

13. ABSTRACT

The existing analytical solutions for gas lubricated stepped sector thrust bearings are reviewed. An experiment performed at high bearing numbers (123 to 165) using air at atmospheric pressure is described. Results are presented of tests conducted using a bearing optimized by the methods of Ausman and Wildmann for high speed operation. Most of the design optimizations are confirmed for high bearing numbers; the exception is load carrying capacity. The load capacity curve obtained takes the same form as that predicted by theory but is lower for any given bearing number by a constant percentage. This points to a need for re-evaluation of determination of load carrying capacity.

DD FORM 1 JAN 64 1473

14. KEY WORDS	LINK A		LINK B		LINK C	
	ROLE	WT	ROLE	WT	ROLE	WT
Bearing						
Thrust						
Gas						
Lubrication						
Step						
Stepped						
Sector						
Experimental						

thesS8575
DUDLEY KNOX LIBRARY
3 2768 00414849 4
DUDLEY KNOX LIBRARY